COMMUN. MATH. SCI.
Vol. 22, No. 6, pp. 1657–1684

AN EFFICIENT INTERFACE HYDROSTATIC RECONSTRUCTION FOR THE TWO-LAYER SHALLOW FLOWS WITH ARBITRARY WET-DRY FRONTS*

JIAN DONG† AND DINGFANG LI‡

Abstract. This paper aims to propose a well-balanced positivity-preserving numerical scheme for the two-layer shallow water systems with arbitrary wet-dry fronts based on interface hydrostatic reconstructions (IHR). One key difficulty in solving the two-layer shallow water systems is the nonconservative product term which can not be evaluated on the cell boundaries. Another difficulty is that the well-balanced property for the still water maybe missed when the computational domain has wet-dry fronts, especially, the wet-dry front is located at the discontinuous bottom topography. For the nonlinear stability of the numerical scheme, the positivity of the water height is vital. To this end, we discretize the nonconservative product term based on the IHR method, which is a particular choice of path-conservative methods. The intermediate bottom level used in the discretization of the bed source term of two layers is different. The nonconservative product term due to the momentum exchange between two layers is discretized using the intermediate interface water height.

The resulting numerical scheme can preserve the positivity of two-layered heights and maintain the still water even when the computational domain has wet-dry fronts. The numerical scheme performs well in solving the complex problems, such as the Kelvin - Helmholtz instable problems. We demonstrate these properties of the current scheme through several classical problems of the two-layer shallow water systems with arbitrary wet-dry fronts.

Keywords. Well-balanced; Positivity preserving; Arbitrary wet-dry fronts; Two-layer shallow water systems; Interface hydrostatic reconstruction.

AMS subject classifications. 76M12; 35L65.

1. Introduction

We propose an efficient second-order accurate, well-balanced, and positivity-preserving numerical scheme for the two-layer shallow water equations with arbitrary wet-dry fronts. It is a challenging task to address the nonconservative product term appearing in the two-layer shallow water systems, because these nonconservative product terms can not be well defined in the distributional framework. Several mathematical theories have been proposed in [26,27]. These nonconservative product terms can be seen as the Borel measures introduced in [26], which are used to define the path-conservative numerical scheme to address these difficulties. However, a disadvantage of the path-conservative schemes is that they depend on the choice of a family of paths in the phase space. Here we propose a path-conservative method based on a suitable choice of the path based on a hydrostatic reconstruction (HR). The first HR method was proposed in Audusse et al. [5], which is well-balanced, positivity-preserving and semi-discrete in-cell entropy satisfying. Unfortunately, Audusse's HR method can not correctly reflect the acceleration due to the sloped bottom topography on a large discrete level. There are several numerical methods to improve Audusse's HR method. We refer to [11, 16] and references therein (obviously, we do not show all the associated references).

We consider the one-dimensional two-layer shallow water system with a nonflat

*Received: May 04, 2021; Accepted (in revised form): January 25, 2024. Communicated by Giovanni Russo.

†Department of Mathematics, College of Science, National University of Defense Technology, Changsha, Hunan, 410073, China (j.dong@whu.edu.cn).

‡School of Mathematics and Statistics, Wuhan University, Wuhan 430072, China (dfli@whu.edu.cn).

bottom topography, which was proposed in [24]:

$$\begin{cases} (h_1)_t + (h_1u_1)_x = 0, \\ (h_1u_1)_t + \left[h_1u_1^2 + \frac{1}{2}g(h_1)^2\right]_x = -gh_1z_x - gh_1(h_2)_x, \\ (h_2)_t + (h_2u_2)_x = 0, \\ (h_2u_2)_t + \left[h_2u_2^2 + \frac{1}{2}g(h_2)^2\right]_x = -gh_2z_x - gh_2(\widetilde{h}_1)_x, \end{cases} \tag{1.1}$$

where h_1 (upper layer) and h_2 (lower layer) represents the height of the layer, $u_i, i=1,2$ denote the fluid velocity, g is the acceleration because of the gravity, the function $z(x)$ denotes the bottom topography. We define $\widetilde{h}_1 = rh_1$, where $r := \frac{\rho_1}{\rho_2}$ is the constant density ratio. The system (1.1) admits the steady-state solution:

$$u_i = 0, \quad w := h_2 + z = const, \quad E := h_1 + h_2 + z = const., \quad i = 1,2, \tag{1.2}$$

where w represents the interface between the upper layer and the lower layer, E denotes the total water level.

A key difficulty of a numerical scheme for the system (1.1) is the discretization of the bed slope source term, which should be exactly balanced by the nonzero flux gradients for the still water even when the computational domain has wet-dry fronts. To shorten the notations, we first rewrite the system (1.1) in a compact form

$$\frac{\partial}{\partial t}\mathbf{U} = -\frac{\partial}{\partial x}\mathbf{F} + \mathbf{S}(\mathbf{U}, z), \tag{1.3}$$

where

$$\mathbf{U} = \begin{pmatrix} h_1 \\ h_1u_1 \\ h_2 \\ h_2u_2 \end{pmatrix}, \quad \mathbf{F}(\mathbf{U}) = \begin{pmatrix} h_1u_1 \\ h_1u_1^2 + \frac{1}{2}gh_1^2 \\ h_2u_2 \\ h_2u_2^2 + \frac{1}{2}gh_2^2 \end{pmatrix}, \quad \mathbf{S}(\mathbf{U}, z) = \begin{pmatrix} 0 \\ -gh_1z_x - gh_1(h_2)_x \\ 0 \\ -gh_2z_x - gh_2(\widetilde{h}_1)_x \end{pmatrix}. \tag{1.4}$$

A well-balanced scheme can preserve the steady state (1.2) at a discrete level. For examples of the well-balanced schemes for the shallow water equation refer to [3, 4, 7, 9, 14, 15, 30] and references therein. A numerical scheme should preserve the physical non-negative water height, because of the calculation of the Jacobian matrix of the flux function. For examples of positivity-preserving schemes refer to [3, 7, 11, 15, 30] and references therein.

Castro-Díaz et al. [23] proposed a path-conservative numerical scheme for solving the two-layer shallow water system. It is worth mentioning that any method, in which the small scale effects (the vanishing diffusion and/or dispersion) are not taken into account, regardless of whether it is path-conservative or not, will not converge to the correct weak solutions when solving the equation with nonconservative products. There are several methods to solve this difficulty, such as, the Glimm or front-tracking methods; or controlled viscosity methods based on the equivalent equation etc. In [31], a path-conservative central-upwind scheme for the two-layer shallow water equation with nonconservative products was proposed. An entropy satisfying time-splitting method was proposed in Bouchut and Luna [19], but their scheme lacks conservation of the total momentum, which leads to a wrong shock at the interface. In [20], they solved this problem and proposed a robust numerical scheme which is positive and well-balanced. Abgrall and Karni [22] proposed a relaxation approach for the one-dimensional two-layer shallow water equations. They discussed the stability of the model. In [34], they

pointed out that a careful numerical treatment of nonconservative products is crucial for designing a robust and highly accurate numerical method. A robust and well-balanced numerical scheme for the two-layer shallow water equations based on a modified HLL flux formulation was proposed in Lu et al. [21]. A discontinuous Galerkin method for two-layer shallow water equations was proposed in Izem et al. [25]. Chiapolino and Saurel [28] constructed a new model of the two-layer shallow water system to address the lack of hyperbolicity.

In this paper, we propose a second-order well-balanced and positivity-preserving central scheme (due to the use of Lax-Friedrichs numerical fluxes) for one-dimensional two-layer shallow water equations with wet-dry fronts. The discretization of the source term is based on subcell reconstructions. The first-order hydrostatic reconstruction based on subcell reconstructions for the single layer shallow water equations was proposed in Chen and Noelle [11]. We reconstruct the total water level, the depth-averaged velocity, and two-layered heights. This reconstruction can preserve the positivity of two-layered heights and guarantee that the wet-dry fronts are located at the cell boundary.

The paper is organized as follows. In Section 2, we introduce a second-order well-balanced positivity-preserving finite volume scheme for the two-layer shallow water equations with source term. We prove that the current scheme can preserve the stationary solution and the positivity of two-layered heights in Section 3. We present several numerical experiments to demonstrate the properties of our numerical method in Section 4. A conclusion follows in Section 5.

2. The numerical method

In this section, we introduce a second-order Godunov-type central scheme for the two-layer shallow water flows with a nonflat bottom topography. We first denote by $C_j=\left[x_{j-\frac{1}{2}},x_{j+\frac{1}{2}}\right]$ the uniform cell to discretize the computational domain. The mesh size is $\Delta x=x_{j+\frac{1}{2}}-x_{j-\frac{1}{2}}$. We denote by $\overline{\mathbf{U}}_j(t)$ the approximate cell average of the solution:

$$\overline{\mathbf{U}}_j(t)\approx\frac{1}{\Delta x}\int_{x_{j-\frac{1}{2}}}^{x_{j+\frac{1}{2}}}\mathbf{U}(x,t)dx.$$

The second-order semi-discretization of the system (1.3) can be written as follows:

$$\frac{d}{dt}\overline{\mathbf{U}}_j(t)=\mathbf{R}(t):=-\frac{1}{\Delta x}\left(\mathbf{F}_{j+\frac{1}{2}}-\mathbf{F}_{j-\frac{1}{2}}\right)+\frac{1}{\Delta x}\left(\mathbf{S}_{j-\frac{1}{2}+}+\mathbf{S}_j+\mathbf{S}_{j+\frac{1}{2}-}\right),\tag{2.1}$$

where $\mathbf{R}$ denotes the residuum, $\mathbf{F}_{j+\frac{1}{2}}:=\overrightarrow{\mathcal{F}}\left(\mathbf{U}_{j+\frac{1}{2}-},\mathbf{U}_{j+\frac{1}{2}+}\right)$ is a numerical flux function which coincides with the true flux, and

$$\mathbf{S}_{j-\frac{1}{2}+}+\mathbf{S}_j+\mathbf{S}_{j+\frac{1}{2}-}\approx\int_{x_{j-\frac{1}{2}}}^{x_{j+\frac{1}{2}}}\mathbf{S}(\mathbf{U},z)dx,$$

denotes the discretization of the source term. We construct a piecewise linear function endowed with a nonlinear limiter in C_j to approximate the exact solution for obtaining the second-order non-oscillatory properties. We reconstruct the variables $\mathbf{q}=(E,h_1,h_2,u_1,u_2)$ instead of $\mathbf{U}$ to preserve the static solution (1.2).

For simplicity, we omit the notation t. The piecewise linear approximate solution reads as follows,

$$\mathbf{q}_j(x):=\overline{\mathbf{q}}_j+(x-x_j)(\overline{\mathbf{q}}_j)',\quad x\in C_j,\tag{2.2}$$

where $(\overline{\mathbf{q}}_j)'$ denotes the first-order approximate spatial derivative of the solution. We choose the minmod function (see [1, 6, 8, 10] and references therein) to calculate the numerical derivative $(\overline{\mathbf{q}}_j)'$:

$$(\overline{\mathbf{q}}_j)' = \text{minmod}\left(\theta\frac{\overline{\mathbf{q}}_j - \overline{\mathbf{q}}_{j-1}}{\Delta x}, \frac{\overline{\mathbf{q}}_{j+1} - \overline{\mathbf{q}}_{j-1}}{2\Delta x}, \theta\frac{\overline{\mathbf{q}}_{j+1} - \overline{\mathbf{q}}_j}{\Delta x}\right), \quad \theta \in [1,2], \tag{2.3}$$

where

$$\text{minmod}(x_1, x_2, x_3, ...) = \begin{cases} \text{sign}(x_j)\min(|x_j|), & \text{if } x_j, \forall j \in \mathbb{Z}, \text{have the same sign}, \\ 0, & \text{otherwise}, \end{cases} \tag{2.4}$$

and θ is a parameter that controls the numerical viscosity of the numerical scheme. Let us remark that the approximate spatial derivative of the interface w is computed by

$$(\overline{w}_j)' = (\overline{E}_j)' - (\overline{(h_1)}_j)'. \tag{2.5}$$

Using the Equation (2.2), we compute the left- and right-sided values of the solution at the cell interface,

$$\begin{aligned} \mathbf{q}_{j+\frac{1}{2}+} &= \overline{\mathbf{q}}_{j+1} - \frac{\Delta x}{2}(\overline{\mathbf{q}}_{j+1})', \quad \mathbf{q}_{j+\frac{1}{2}-} = \overline{\mathbf{q}}_j + \frac{\Delta x}{2}(\overline{\mathbf{q}}_j)', \\ w_{j+\frac{1}{2}+} &= E_{j+\frac{1}{2}+} - (h_1)_{j+\frac{1}{2}+}, \quad w_{j+\frac{1}{2}-} = E_{j+\frac{1}{2}-} - (h_1)_{j+\frac{1}{2}-}, \\ z_{j+\frac{1}{2}+} &= w_{j+\frac{1}{2}+} - (h_2)_{j+\frac{1}{2}+}, \quad z_{j+\frac{1}{2}-} = w_{j+\frac{1}{2}-} - (h_2)_{j+\frac{1}{2}-}. \end{aligned} \tag{2.6}$$

Next, we use the hydrostatic reconstruction method proposed in [11] to define the intermediate bottom level and the intermediate layered heights as,

$$\begin{aligned} z_{j+\frac{1}{2}} &= \min\left(\max\left(z_{j+\frac{1}{2}-}, z_{j+\frac{1}{2}+}\right), \min\left(E_{j+\frac{1}{2}-}, E_{j+\frac{1}{2}+}\right)\right), \\ (h_1)^*_{j+\frac{1}{2}-} &= \min\left(E_{j+\frac{1}{2}-} - z_{j+\frac{1}{2}}, (h_1)_{j+\frac{1}{2}-}\right), \\ (h_1)^*_{j+\frac{1}{2}+} &= \min\left(E_{j+\frac{1}{2}+} - z_{j+\frac{1}{2}}, (h_1)_{j+\frac{1}{2}+}\right), \\ (h_2)^*_{j+\frac{1}{2}-} &= \min\left(w_{j+\frac{1}{2}-} - z_{j+\frac{1}{2}}, (h_2)_{j+\frac{1}{2}-}\right), \\ (h_2)^*_{j+\frac{1}{2}+} &= \min\left(w_{j+\frac{1}{2}+} - z_{j+\frac{1}{2}}, (h_2)_{j+\frac{1}{2}+}\right), \end{aligned} \tag{2.7}$$

and the *interface intermediate layered heights* are defined as

$$\begin{aligned} (h_1)_{j+\frac{1}{2}} &= \frac{1}{2}\left((h_1)^*_{j+\frac{1}{2}-} + (h_1)^*_{j+\frac{1}{2}+}\right), \\ (h_2)_{j+\frac{1}{2}} &= \frac{1}{2}\left((h_2)^*_{j+\frac{1}{2}-} + (h_2)^*_{j+\frac{1}{2}+}\right). \end{aligned} \tag{2.8}$$

The intermediate discharge $(hu)^*_{j+\frac{1}{2}\pm}$ at the point $x_{j+\frac{1}{2}}$ is computed by

$$(h_1u_1)^*_{j+\frac{1}{2}\pm} = (h_1)^*_{j+\frac{1}{2}\pm}(u_1)_{j+\frac{1}{2}\pm}, \quad (h_2u_2)^*_{j+\frac{1}{2}\pm} = (h_2)^*_{j+\frac{1}{2}\pm}(u_2)_{j+\frac{1}{2}\pm}. \tag{2.9}$$

We use the method from [2] to compute the velocity,

$$(\overline{u_1})_j = \begin{cases} \frac{(\overline{h_1u_1})_j}{(\overline{h_1})_j}, & \text{if } (\overline{h_1})_j > \varepsilon, \\ 0, & \text{otherwise}, \end{cases} \quad (\overline{u_2})_j = \begin{cases} \frac{(\overline{h_2u_2})_j}{(\overline{h_2})_j}, & \text{if } (\overline{h_2})_j > \varepsilon, \\ 0, & \text{otherwise}, \end{cases} \tag{2.10}$$

where $\varepsilon = 10^{-9}$ is a threshold value of a dry cell.

REMARK 2.1. We would like to stress that (i) the reconstruction in (2.6) can guarantee the positivity of limited values of two-layered heights because of the maximum principle for $\theta \le 2$; (ii) The Equation (2.8) is necessary to mitigate the Kelvin - Helmholtz instability.

2.1. Modification at the wet-dry fronts. The definition of the intermediate states in (2.7) can not preserve the still water when the computational domain has wet-dry fronts. To overcome this difficulty, we need to redefine the intermediate states.

When the cell interface has the wet-dry front, i.e.

$$\max\left(z_{j+\frac{1}{2}-},z_{j+\frac{1}{2}+}\right)>\min\left(E_{j+\frac{1}{2}-},E_{j+\frac{1}{2}+}\right), \tag{2.11}$$

or

$$\min\left(w_{j+\frac{1}{2}-},w_{j+\frac{1}{2}+}\right)<\max\left(z_{j+\frac{1}{2}-},z_{j+\frac{1}{2}+}\right)<\min\left(E_{j+\frac{1}{2}-},E_{j+\frac{1}{2}+}\right), \tag{2.12}$$

we then use the following method. We first define $\widehat{z}_{j+\frac{1}{2}}=z_{j+\frac{1}{2}}$, and then

→ If $z_{j+\frac{1}{2}-}>z_{j+\frac{1}{2}+}$, we modify the intermediate bottom level and the intermediate values of the height of the lower layer as

$$\begin{aligned}\widehat{z}_{j+\frac{1}{2}}&=\min\left(\max\left(z_{j+\frac{1}{2}-},z_{j+\frac{1}{2}+}\right),\min\left(w_{j+\frac{1}{2}-},w_{j+\frac{1}{2}+}\right)\right),\\(h_2)^*_{j+\frac{1}{2}-}&=\min\left(w_{j+\frac{1}{2}-}-\widehat{z}_{j+\frac{1}{2}},(h_2)_{j+\frac{1}{2}-}\right),\\(h_2)^*_{j+\frac{1}{2}+}&=\max\left(w_{j+\frac{1}{2}+}-\widehat{z}_{j+\frac{1}{2}},0\right),\end{aligned} \tag{2.13}$$

→ If $z_{j+\frac{1}{2}-}<z_{j+\frac{1}{2}+}$, we modify the intermediate bottom level and the intermediate values of the height of the lower layer as

$$\begin{aligned}\widehat{z}_{j+\frac{1}{2}}&=\min\left(\max\left(z_{j+\frac{1}{2}-},z_{j+\frac{1}{2}+}\right),\min\left(w_{j+\frac{1}{2}-},w_{j+\frac{1}{2}+}\right)\right),\\(h_2)^*_{j+\frac{1}{2}-}&=\max\left(w_{j+\frac{1}{2}-}-\widehat{z}_{j+\frac{1}{2}},0\right),\\(h_2)^*_{j+\frac{1}{2}+}&=\min\left(w_{j+\frac{1}{2}+}-\widehat{z}_{j+\frac{1}{2}},(h_2)_{j+\frac{1}{2}+}\right).\end{aligned} \tag{2.14}$$

REMARK 2.2. The condition (2.11) corresponds to the case where the upper layer has the wet-dry front. The condition (2.12) corresponds to the case where the lower layer has the wet-dry front while the upper layer is the fully wet case.

2.2. The numerical fluxes. The numerical flux was obtained by the simple local Lax-Friedrichs flux,

$$\begin{aligned}\mathbf{F}_{j+\frac{1}{2}}&:=\overrightarrow{\mathcal{F}}\left(\mathbf{U}^*_{j+\frac{1}{2}-},\mathbf{U}^*_{j+\frac{1}{2}+}\right)\\&=\frac{1}{2}\left(\mathbf{F}\left(\mathbf{U}^*_{j+\frac{1}{2}-}\right)+\mathbf{F}\left(\mathbf{U}^*_{j+\frac{1}{2}+}\right)-\alpha_{j+\frac{1}{2}}\left(\mathbf{U}^*_{j+\frac{1}{2}+}-\mathbf{U}^*_{j+\frac{1}{2}-}\right)\right),\end{aligned} \tag{2.15}$$

where $\alpha_{j+\frac{1}{2}}$ is computed by

$$\begin{aligned}&\alpha_{j+\frac{1}{2}}=\max(\alpha_1,\alpha_2,\alpha_3,\alpha_4),\\&\alpha_1=\left|(u_1)_{j+\frac{1}{2}-}\right|+\sqrt{g\left(1+\sqrt{r}\right)\left((h_1)^*_{j+\frac{1}{2}-}+(h_2)^*_{j+\frac{1}{2}-}\right)}\\&\alpha_2=\left|(u_1)_{j+\frac{1}{2}+}\right|+\sqrt{g\left(1+\sqrt{r}\right)\left((h_1)^*_{j+\frac{1}{2}+}+(h_2)^*_{j+\frac{1}{2}+}\right)}\\&\alpha_3=\left|(u_2)_{j+\frac{1}{2}-}\right|+\sqrt{g\left(1+\sqrt{r}\right)\left((h_1)^*_{j+\frac{1}{2}-}+(h_2)^*_{j+\frac{1}{2}-}\right)}\\&\alpha_4=\left|(u_2)_{j+\frac{1}{2}+}\right|+\sqrt{g\left(1+\sqrt{r}\right)\left((h_1)^*_{j+\frac{1}{2}+}+(h_2)^*_{j+\frac{1}{2}+}\right)}.\end{aligned} \tag{2.16}$$

We refer to [22] for more details associated with the estimate of the local speeds. The Lax-Friedrichs flux satisfies the conservativeness and consistency.

2.3. Weak solutions of the nonconservative product terms. This section interprets the numerical method which belongs to a class of *path-conservative* numerical schemes. We first give the definition of the chosen path which satisfies several local Lipschitz conditions (see [12,13,31,32] and references therein).

DEFINITION 2.1. *A family of paths in an open convex subset Ω of $\mathbf{R}^N$ is a locally Lipschitz map*

$$\mathbf{\Phi}:[0,1]\times\Omega\times\Omega\to\Omega,$$

such that:

♯ $\mathbf{\Phi}(0;\mathbf{U}_l,\mathbf{U}_r)=\mathbf{U}_l$ *and* $\mathbf{\Phi}(1;\mathbf{U}_l,\mathbf{U}_r)=\mathbf{U}_r$, $\forall\,\mathbf{U}_l,\mathbf{U}_r\in\Omega$.

♯ *For every arbitrary bounded set $\mathcal{O}\subset\Omega$, there exists a constant k such that*

$$\left|\frac{\partial\mathbf{\Phi}}{\partial s}(s;\mathbf{U}_l,\mathbf{U}_r)\right|\le k|\mathbf{U}_l-\mathbf{U}_r|, \tag{2.17}$$

for any $\mathbf{U}_l,\mathbf{U}_r\in\mathcal{O}$ and almost every $s\in[0,1]$.

♯ *For every arbitrary bounded set $\mathcal{O}\subset\Omega$, there exists a constant K such that*

$$\left|\frac{\partial\mathbf{\Phi}}{\partial s}(s;\mathbf{U}_l^1,\mathbf{U}_r^1)-\frac{\partial\mathbf{\Phi}}{\partial s}(s;\mathbf{U}_l^2,\mathbf{U}_r^2)\right|\le K\left(|\mathbf{U}_l^1-\mathbf{U}_l^2|+|\mathbf{U}_r^1-\mathbf{U}_r^2|\right), \tag{2.18}$$

for any $\mathbf{U}_l^1,\mathbf{U}_r^1,\mathbf{U}_l^2,\mathbf{U}_r^2\in\mathcal{O}$ and almost every $s\in[0,1]$.

We rewrite the system (1.3) as follows

$$\widetilde{\mathbf{U}}_t+\widetilde{A}(\widetilde{\mathbf{U}})\widetilde{\mathbf{U}}_x=0,$$

where, $\widetilde{\mathbf{U}}:=(\mathbf{U},z)^\top$ and

$$\widetilde{A}(\widetilde{\mathbf{U}})=\begin{pmatrix}\frac{\partial\mathbf{F}(\mathbf{U})}{\partial\mathbf{U}}-\mathbf{B}(\mathbf{U}) & -\mathbf{S}(\mathbf{U})\\ 0 & 0\end{pmatrix},$$

and

$$\mathbf{B}(\mathbf{U})=\begin{pmatrix}0&0&0&0\\0&0&-gh_1&0\\0&0&0&0\\-grh_2&0&0&0\end{pmatrix},\quad \mathbf{S}(\mathbf{U})=\begin{pmatrix}0\\-gh_1\\0\\-gh_2\end{pmatrix}.$$

As discussed in [13], the nonconservative product term $\widetilde{A}(\widetilde{\mathbf{U}})\widetilde{\mathbf{U}}_x$ can be interpreted as a Borel's measure that depends on the family of paths in the phase space.

DEFINITION 2.2. *Assume that the solution $\widetilde{\mathbf{U}}(x,t)$ is a regular piecewise weak solution. The Borel's measure denoted by $<[\widetilde{A}(\widetilde{\mathbf{U}}(\cdot,t))\widetilde{\mathbf{U}}(\cdot,t)_x]_{\mathbf{\Phi}},\varphi>$ related to the nonconservative product term $\widetilde{A}(\widetilde{\mathbf{U}})\widetilde{\mathbf{U}}_x$ can be defined as*

$$\begin{aligned}<[\widetilde{A}(\widetilde{\mathbf{U}})\widetilde{\mathbf{U}}_x]_{\mathbf{\Phi}},\varphi>=&\int_R\widetilde{A}(\widetilde{\mathbf{U}}(x,t))\widetilde{\mathbf{U}}(x,t)_x\varphi(x)dx\\&+\sum_i\left(\int_0^1\widetilde{A}(\mathbf{\Phi}(s;\widetilde{\mathbf{U}}_l^i,\widetilde{\mathbf{U}}_r^i))\frac{\partial}{\partial s}\mathbf{\Phi}(s;\widetilde{\mathbf{U}}_l^i,\widetilde{\mathbf{U}}_r^i)ds\right)\varphi(x_i(t)),\end{aligned} \tag{2.19}$$

here $x_i(t)$ denotes the discontinuity of the solution at the time t and $\varphi(x)$ is a smooth function with compact support. The notations $\widetilde{\mathbf{U}}_l^i$ and $\widetilde{\mathbf{U}}_r^i$ are the left and right limit of $\widetilde{\mathbf{U}}$ at the point $x_i(t)$, respectively.

In [33], they proposed a new concept of the high-order path-conservative scheme for interpreting the hydrostatic reconstruction methods [5] and introducing *general hydrostatic reconstruction* methods. We first introduce the new concept of the high-order path-conservative scheme.

$$\frac{d}{dt}\overline{\mathbf{U}}_j(t) = -\frac{1}{\Delta x}\left(\mathbf{E}_{j-\frac{1}{2}+} + \mathbf{E}_{j+\frac{1}{2}-} + \int_{C_j} \widetilde{\mathbf{A}}(\mathbf{q}_j(x))\frac{d\mathbf{q}_j(x)}{dx}dx\right), \tag{2.20}$$

here

$$\begin{aligned}
\mathbf{E}_{j+\frac{1}{2}-} &= \mathbf{D}_{j+\frac{1}{2}-} + \int_0^1 \widetilde{\mathbf{A}}\left(\mathbf{\Phi}^{-,*}(s;\widetilde{\mathbf{U}}_{j+\frac{1}{2}-}, \widetilde{\mathbf{U}}^*_{j+\frac{1}{2}-})\right)\frac{d\mathbf{\Phi}^{-,*}\left(s;\widetilde{\mathbf{U}}_{j+\frac{1}{2}-}, \widetilde{\mathbf{U}}^*_{j+\frac{1}{2}-}\right)}{ds}ds,\\
\mathbf{E}_{j+\frac{1}{2}+} &= \mathbf{D}_{j+\frac{1}{2}+} + \int_0^1 \widetilde{\mathbf{A}}\left(\mathbf{\Phi}^{+,*}(s;\widetilde{\mathbf{U}}_{j+\frac{1}{2}+}, \widetilde{\mathbf{U}}^*_{j+\frac{1}{2}+})\right)\frac{d\mathbf{\Phi}^{+,*}\left(s;\widetilde{\mathbf{U}}_{j+\frac{1}{2}+}, \widetilde{\mathbf{U}}^*_{j+\frac{1}{2}+}\right)}{ds}ds,
\end{aligned} \tag{2.21}$$

and

$$\mathbf{D}_{j+\frac{1}{2}\pm} = \mathbf{D}_{j+\frac{1}{2}\pm}(\widetilde{\mathbf{U}}^*_{j+\frac{1}{2}-}, \widetilde{\mathbf{U}}^*_{j+\frac{1}{2}+}), \tag{2.22}$$

and

$$\mathbf{\Phi}^{\pm,*} = \begin{pmatrix} \mathbf{\Phi}_h^{\pm,*} \\ \Phi_z^{\pm} \end{pmatrix}, \quad \mathbf{\Phi}_h^{\pm,*} = \begin{pmatrix} \mathbf{\Phi}_{h_1}^{\pm,*} \\ \mathbf{\Phi}_{h_1u_1}^{\pm,*} \\ \mathbf{\Phi}_{h_2}^{\pm,*} \\ \mathbf{\Phi}_{h_2u_2}^{\pm,*} \end{pmatrix}. \tag{2.23}$$

It is worth mentioning that the Dirac measure satisfies the following consistency properties.

$$\mathbf{D}_{j+\frac{1}{2}\pm}(\widetilde{\mathbf{U}}, \widetilde{\mathbf{U}}) = 0, \tag{2.24}$$

and

$$\mathbf{D}_{j+\frac{1}{2}-} + \mathbf{D}_{j+\frac{1}{2}+} = \int_0^1 \widetilde{A}\left(\mathbf{\Phi}(s;\widetilde{\mathbf{U}}^*_{j+\frac{1}{2}-}, \widetilde{\mathbf{U}}^*_{j+\frac{1}{2}+})\right)\frac{\partial}{\partial s}\mathbf{\Phi}\left(s;\widetilde{\mathbf{U}}^*_{j+\frac{1}{2}-}, \widetilde{\mathbf{U}}^*_{j+\frac{1}{2}+}\right)ds. \tag{2.25}$$

In [13], they discussed the relations between the conservative and path-conservative schemes. Using the concept of new path-conservative schemes (2.20)-(2.25) proposed in [33], we rewrite the Equation (2.1) as

$$\frac{d}{dt}\overline{\mathbf{U}}_j(t) = -\frac{1}{\Delta x}\left(\mathbf{E}_{j-\frac{1}{2}+} + \mathbf{E}_{j+\frac{1}{2}-} + \mathbf{F}(\mathbf{U}_{j+\frac{1}{2}-}) - \mathbf{F}(\mathbf{U}_{j-\frac{1}{2}+}) - \mathbf{S}_j\right), \tag{2.26}$$

here

$$\begin{aligned}
\mathbf{E}_{j+\frac{1}{2}-} &:= \mathbf{F}_{j+\frac{1}{2}} - \mathbf{F}(\mathbf{U}_{j+\frac{1}{2}-}) - \mathbf{S}_{j+\frac{1}{2}-},\\
\mathbf{E}_{j-\frac{1}{2}+} &:= \mathbf{F}(\mathbf{U}_{j-\frac{1}{2}+}) - \mathbf{F}_{j-\frac{1}{2}} - \mathbf{S}_{j-\frac{1}{2}+}.
\end{aligned} \tag{2.27}$$

We have used the following relations:

$$\begin{aligned}\mathbf{D}_{j+\frac{1}{2}-} :=& \mathbf{F}_{j+\frac{1}{2}} - \mathbf{F}(\mathbf{U}_{j+\frac{1}{2}-}),\\ \mathbf{D}_{j-\frac{1}{2}+} :=& \mathbf{F}(\mathbf{U}_{j-\frac{1}{2}+}) - \mathbf{F}_{j-\frac{1}{2}}.\end{aligned}$$

It is worth pointing out that the term $\mathbf{S}_{j+\frac{1}{2}\pm}$ and $\mathbf{S}_j$ can be computed as

$$\begin{aligned}\mathbf{S}_{j-\frac{1}{2}+} =& \int_0^1 \mathbf{B}(\mathbf{\Phi}_h^{+,*}(s;\mathbf{U}_{j-\frac{1}{2}+},\mathbf{U}^*_{j-\frac{1}{2}+}))\frac{\partial}{\partial s}\mathbf{\Phi}_h^{+,*}(s;\mathbf{U}_{j-\frac{1}{2}+},\mathbf{U}^*_{j-\frac{1}{2}+})ds\\ &+\int_0^1 \mathbf{S}(\mathbf{\Phi}_h^{+,*}(s;\mathbf{U}_{j-\frac{1}{2}+},\mathbf{U}^*_{j-\frac{1}{2}+}))\frac{\partial}{\partial s}\Phi_z^{+}(s;z_{j-\frac{1}{2}+},\widehat{z}_{j-\frac{1}{2}})ds,\\ \mathbf{S}_{j+\frac{1}{2}-} =& \int_0^1 \mathbf{B}(\mathbf{\Phi}_h^{-,*}(s;\mathbf{U}_{j+\frac{1}{2}-},\mathbf{U}^*_{j+\frac{1}{2}-}))\frac{\partial}{\partial s}\mathbf{\Phi}_h^{-,*}(s;\mathbf{U}_{j+\frac{1}{2}-},\mathbf{U}^*_{j+\frac{1}{2}-})ds\\ &+\int_0^1 \mathbf{S}(\mathbf{\Phi}_h^{-,*}(s;\mathbf{U}_{j+\frac{1}{2}-},\mathbf{U}^*_{j+\frac{1}{2}-}))\frac{\partial}{\partial s}\Phi_z^{-}(s;z_{j+\frac{1}{2}-},\widehat{z}_{j+\frac{1}{2}})ds,\\ \mathbf{S}_j =& \int_{C_j}\mathbf{B}(\mathbf{U})\frac{\partial}{\partial x}\mathbf{U}dx + \int_{C_j}\mathbf{S}(\mathbf{U})\frac{\partial}{\partial x}z(x)dx.\end{aligned} \tag{2.28}$$

Let us remark that the scheme (2.26) coupled with the discretization of the nonconservative product term (2.28) cannot correctly reflect the Kelvin-Helmholtz instable phenomenona which can be seen in the numerical examples. For overcoming this issue, we discretize the nonconservative product term using the following paths.

$$\begin{aligned}\mathbf{S}_{j-\frac{1}{2}+} =& \int_0^1 \mathbf{B}(\mathbf{\Phi}_h^{+,*}(s;\mathbf{U}_{j-\frac{1}{2}+},\mathbf{U}^*_{j-\frac{1}{2}+}))\frac{\partial}{\partial s}\mathbf{\Phi}_h^{+}(s;\mathbf{U}_{j-\frac{1}{2}+},\mathbf{U}_{j-\frac{1}{2}})ds\\ &+\int_0^1 \mathbf{S}(\mathbf{\Phi}_h^{+,*}(s;\mathbf{U}_{j-\frac{1}{2}+},\mathbf{U}^*_{j-\frac{1}{2}+}))\frac{\partial}{\partial s}\Phi_z^{+}(s;z_{j-\frac{1}{2}+},\widehat{z}_{j-\frac{1}{2}})ds,\\ \mathbf{S}_{j+\frac{1}{2}-} =& \int_0^1 \mathbf{B}(\mathbf{\Phi}_h^{-,*}(s;\mathbf{U}_{j+\frac{1}{2}-},\mathbf{U}^*_{j+\frac{1}{2}-}))\frac{\partial}{\partial s}\mathbf{\Phi}_h^{-}(s;\mathbf{U}_{j+\frac{1}{2}-},\mathbf{U}_{j+\frac{1}{2}})ds\\ &+\int_0^1 \mathbf{S}(\mathbf{\Phi}_h^{-,*}(s;\mathbf{U}_{j+\frac{1}{2}-},\mathbf{U}^*_{j+\frac{1}{2}-}))\frac{\partial}{\partial s}\Phi_z^{-}(s;z_{j+\frac{1}{2}-},\widehat{z}_{j+\frac{1}{2}})ds,\\ \mathbf{S}_j =& \int_{C_j}\mathbf{B}(\mathbf{U})\frac{\partial}{\partial x}\mathbf{U}dx + \int_{C_j}\mathbf{S}(\mathbf{U})\frac{\partial}{\partial x}z(x)dx,\end{aligned} \tag{2.29}$$

here, we use the notations

$$\mathbf{\Phi}^{\pm} = \begin{pmatrix}\mathbf{\Phi}_h^{\pm}\\ \Phi_z^{\pm}\end{pmatrix}, \quad \mathbf{\Phi}_h^{\pm} = \begin{pmatrix}\mathbf{\Phi}^{\pm}_{h_1}\\ \mathbf{\Phi}^{\pm}_{h_1u_1}\\ \mathbf{\Phi}^{\pm}_{h_2}\\ \mathbf{\Phi}^{\pm}_{h_2u_2}\end{pmatrix}.$$

The paths will be discussed in latter.

2.3.1. Discretizing the source terms. We choose a straight line to connect the states $\mathbf{Q}^{\pm}_{i+\frac{1}{2}}$ and $\mathbf{Q}^*_{i+\frac{1}{2}\pm}$, which is defined as

$$\begin{aligned}&\mathbf{\Phi}_h^{\pm,*}:[0,1]\times\mathbf{R}^4\times\mathbf{R}^4\to\mathbf{R}^4,\\ &\mathbf{\Phi}_h^{+,*}\left(0;\mathbf{Q}_{i+\frac{1}{2}+},\mathbf{Q}^*_{i+\frac{1}{2}+}\right) = \mathbf{Q}^*_{i+\frac{1}{2}+},\ \mathbf{\Phi}_h^{+,*}\left(1;\mathbf{Q}_{i+\frac{1}{2}+},\mathbf{Q}^*_{i+\frac{1}{2}+}\right) = \mathbf{Q}_{i+\frac{1}{2}+},\\ &\mathbf{\Phi}_h^{-,*}\left(0;\mathbf{Q}_{i+\frac{1}{2}-},\mathbf{Q}^*_{i+\frac{1}{2}-}\right) = \mathbf{Q}_{i+\frac{1}{2}-},\ \mathbf{\Phi}_h^{-,*}\left(1;\mathbf{Q}_{i+\frac{1}{2}-},\mathbf{Q}^*_{i+\frac{1}{2}-}\right) = \mathbf{Q}^*_{i+\frac{1}{2}-},\end{aligned} \tag{2.30}$$

and the smooth path takes the following form,

$$\begin{aligned}\mathbf{\Phi}_h^{+,*}\left(s;\mathbf{Q}_{i+\frac{1}{2}+},\mathbf{Q}^*_{i+\frac{1}{2}+}\right)&=(1-s)\mathbf{Q}^*_{i+\frac{1}{2}+}+s\mathbf{Q}_{i+\frac{1}{2}+},\\ \mathbf{\Phi}_h^{-,*}\left(s;\mathbf{Q}_{i+\frac{1}{2}-},\mathbf{Q}^*_{i+\frac{1}{2}-}\right)&=(1-s)\mathbf{Q}_{i+\frac{1}{2}-}+s\mathbf{Q}^*_{i+\frac{1}{2}-},\end{aligned}\tag{2.31}$$

here, we denote $\mathbf{Q}=(h_1,h_1u_1,h_2,h_2u_2)^\top$.

A straight line connecting the states $\mathbf{Q}^{\pm}_{i+\frac{1}{2}}$ and $\mathbf{Q}_{i+\frac{1}{2}}$ can be defined as

$$\begin{aligned}&\mathbf{\Phi}_h^{\pm}:[0,1]\times\mathbf{R}^4\times\mathbf{R}^4\to\mathbf{R}^4,\\ &\mathbf{\Phi}_h^{+}\left(0;\mathbf{Q}_{i+\frac{1}{2}+},\mathbf{Q}_{i+\frac{1}{2}}\right)=\mathbf{Q}_{i+\frac{1}{2}},\ \mathbf{\Phi}_h^{+}\left(1;\mathbf{Q}_{i+\frac{1}{2}+},\mathbf{Q}_{i+\frac{1}{2}}\right)=\mathbf{Q}_{i+\frac{1}{2}+},\\ &\mathbf{\Phi}_h^{-}\left(0;\mathbf{Q}_{i+\frac{1}{2}-},\mathbf{Q}_{i+\frac{1}{2}}\right)=\mathbf{Q}_{i+\frac{1}{2}-},\ \mathbf{\Phi}_h^{-}\left(1;\mathbf{Q}_{i+\frac{1}{2}-},\mathbf{Q}_{i+\frac{1}{2}}\right)=\mathbf{Q}_{i+\frac{1}{2}},\end{aligned}\tag{2.32}$$

and the smooth path takes the following form,

$$\begin{aligned}\mathbf{\Phi}_h^{+,*}\left(s;\mathbf{Q}_{i+\frac{1}{2}+},\mathbf{Q}_{i+\frac{1}{2}}\right)&=(1-s)\mathbf{Q}_{i+\frac{1}{2}}+s\mathbf{Q}_{i+\frac{1}{2}+},\\ \mathbf{\Phi}_h^{-,*}\left(s;\mathbf{Q}_{i+\frac{1}{2}-},\mathbf{Q}_{i+\frac{1}{2}}\right)&=(1-s)\mathbf{Q}_{i+\frac{1}{2}-}+s\mathbf{Q}_{i+\frac{1}{2}}.\end{aligned}\tag{2.33}$$

A straight line connects the states $z_{i+\frac{1}{2}\pm}$ related to the nonconservative product term that encompasses the bottom topography can be defined as

$$\begin{aligned}&\Phi_z^{\pm}:[0,1]\times R\times R\to R,\\ &\Phi_z^{+}\left(0;z_{i+\frac{1}{2}+},\widehat{z}_{i+\frac{1}{2}}\right)=\widehat{z}_{i+\frac{1}{2}},\ \Phi_z^{+}\left(1;z_{i+\frac{1}{2}+},\widehat{z}_{i+\frac{1}{2}}\right)=z_{i+\frac{1}{2}+},\\ &\Phi_z^{-}\left(0;z_{i+\frac{1}{2}-},\widehat{z}_{i+\frac{1}{2}}\right)=z_{i+\frac{1}{2}-},\ \Phi_z^{-}\left(1;z_{i+\frac{1}{2}-},\widehat{z}_{i+\frac{1}{2}}\right)=\widehat{z}_{i+\frac{1}{2}},\end{aligned}\tag{2.34}$$

and the smooth path takes the following form,

$$\begin{aligned}\Phi_z^{+}\left(s;z_{i+\frac{1}{2}+},z_{i+\frac{1}{2}}\right)&=(1-s)z_{i+\frac{1}{2}}+sz_{i+\frac{1}{2}+},\\ \Phi_z^{-}\left(s;z_{i+\frac{1}{2}-},z_{i+\frac{1}{2}}\right)&=(1-s)z_{i+\frac{1}{2}-}+sz_{i+\frac{1}{2}}.\end{aligned}\tag{2.35}$$

Next, we can give the explicit discretized formulae related to the nonconservative product terms. As an example, we show the discretization of the term $-gh_1(h_2)_x$ and $-gh_1z_x$. We first omit the time notation t^n. According to the Equations (2.19)-(2.33), we compute the integral of the term $-gh_1(h_2)_x$,

$$\begin{aligned}&-\int_{C_j}g(h_1)(x)(h_2)_x dx\\ =&-\int_0^1 g\Phi^+_{h_1}(s;(h_1)_{j-\frac{1}{2}+},(h_1)^*_{j-\frac{1}{2}+})\frac{\partial}{\partial s}\Phi^+_{h_2}(s;(h_2)_{j-\frac{1}{2}+},(h_2)_{j-\frac{1}{2}})ds\\ &-\int_0^1 g\Phi^-_{h_1}(s;(h_1)_{j+\frac{1}{2}-},(h_1)^*_{j+\frac{1}{2}-})\frac{\partial}{\partial s}\Phi^-_{h_2}(s;(h_2)_{j+\frac{1}{2}-},(h_2)_{j+\frac{1}{2}})ds\\ &-\int_{C_j}g(h_1)_j(x)(((h_2)_j)_x)(x)dx\\ =&-\frac{1}{2}g\left((h_1)_{j-\frac{1}{2}+}+(h_1)^*_{j-\frac{1}{2}+}\right)\left((h_2)_{j-\frac{1}{2}+}-(h_2)_{j-\frac{1}{2}}\right),\end{aligned}$$

$$-\frac{1}{2}g\Big((h_1)^*_{j+\frac{1}{2}-}+(h_1)_{j+\frac{1}{2}-}\Big)\Big((h_2)_{j+\frac{1}{2}}-(h_2)_{j+\frac{1}{2}-}\Big),$$
$$-\frac{1}{2}g\Big((h_1)_{j-\frac{1}{2}+}+(h_1)_{j+\frac{1}{2}-}\Big)\Big((h_2)_{j+\frac{1}{2}-}-(h_2)_{j-\frac{1}{2}+}\Big).$$

According to the Equations (2.19)-(2.33) and (2.35), we compute the integral of the term $-gh_1z_x$,

$$\begin{aligned}
-\int_{C_j} g(h_1)(x)z_x dx =& -\int_0^1 g\Phi^+_{h_1}(s;(h_1)_{j-\frac{1}{2}+},(h_1)^*_{j-\frac{1}{2}+})\frac{\partial}{\partial s}\Phi_z(s;z_{j-\frac{1}{2}-},z_{j-\frac{1}{2}},z_{j-\frac{1}{2}+})ds\\
&-\int_0^1 g\Phi^-_{h_1}(s;(h_1)_{j+\frac{1}{2}-},(h_1)^*_{j+\frac{1}{2}-})\frac{\partial}{\partial s}\Phi_z(s;z_{j+\frac{1}{2}-},z_{j+\frac{1}{2}},z_{j+\frac{1}{2}+})ds\\
&-\int_{C_j} g(h_1)_j(x)((z_j)_x)(x)dx\\
=&-\frac{1}{2}g\Big((h_1)_{j-\frac{1}{2}+}+(h_1)^*_{j-\frac{1}{2}+}\Big)\Big(z_{j-\frac{1}{2}+}-\widehat{z}_{j-\frac{1}{2}}\Big),\\
&-\frac{1}{2}g\Big((h_1)^*_{j+\frac{1}{2}-}+(h_1)_{j+\frac{1}{2}-}\Big)\Big(\widehat{z}_{j+\frac{1}{2}}-z_{j+\frac{1}{2}-}\Big),\\
&-\frac{1}{2}g\Big((h_1)_{j-\frac{1}{2}+}+(h_1)_{j+\frac{1}{2}-}\Big)\Big(z_{j+\frac{1}{2}-}-z_{j-\frac{1}{2}+}\Big).
\end{aligned}$$

The other terms can be computed using the similar method. Finally, we can obtain the discretization of the second component of the source term reads as follows

$$\begin{aligned}
\mathbf{S}^{(2)}_{j-\frac{1}{2}+} &= -\tfrac{1}{2}g\Big((h_1)_{j-\frac{1}{2}+}+(h_1)^*_{j-\frac{1}{2}+}\Big)\Big(z_{j-\frac{1}{2}+}+(h_2)_{j-\frac{1}{2}+}-z_{j-\frac{1}{2}}-(h_2)_{j-\frac{1}{2}}\Big),\\
\mathbf{S}^{(2)}_{j+\frac{1}{2}-} &= -\tfrac{1}{2}g\Big((h_1)^*_{j+\frac{1}{2}-}+(h_1)_{j+\frac{1}{2}-}\Big)\Big(z_{j+\frac{1}{2}}+(h_2)_{j+\frac{1}{2}}-z_{j+\frac{1}{2}-}-(h_2)_{j+\frac{1}{2}-}\Big),\\
\mathbf{S}^{(2)}_{j} &= -\tfrac{1}{2}g\Big((h_1)_{j-\frac{1}{2}+}+(h_1)_{j+\frac{1}{2}-}\Big)\Big(z_{j+\frac{1}{2}-}+(h_2)_{j+\frac{1}{2}-}-z_{j-\frac{1}{2}+}-(h_2)_{j-\frac{1}{2}+}\Big),
\end{aligned}\tag{2.36}$$

and the discretization of the fourth component of the source term reads as follows

$$\begin{aligned}
\mathbf{S}^{(4)}_{j-\frac{1}{2}+} &= -\tfrac{1}{2}g\Big((h_2)_{j-\frac{1}{2}+}+(h_2)^*_{j-\frac{1}{2}+}\Big)\Big(z_{j-\frac{1}{2}+}+(\widetilde{h}_1)^*_{j-\frac{1}{2}+}-\widehat{z}_{j-\frac{1}{2}}-(\widetilde{h}_1)_{j-\frac{1}{2}}\Big),\\
\mathbf{S}^{(4)}_{j+\frac{1}{2}-} &= -\tfrac{1}{2}g\Big((h_2)^*_{j+\frac{1}{2}-}+(h_2)_{j+\frac{1}{2}-}\Big)\Big(\widehat{z}_{j+\frac{1}{2}}+(\widetilde{h}_1)_{j+\frac{1}{2}}-z_{j+\frac{1}{2}-}-(\widetilde{h}_1)^*_{j+\frac{1}{2}-}\Big),\\
\mathbf{S}^{(4)}_{j} &= -\tfrac{1}{2}g\Big((h_2)_{j-\frac{1}{2}+}+(h_2)_{j+\frac{1}{2}-}\Big)\Big(z_{j+\frac{1}{2}-}+(\widetilde{h}_1)_{j+\frac{1}{2}-}-z_{j-\frac{1}{2}+}-(\widetilde{h}_1)_{j-\frac{1}{2}+}\Big).
\end{aligned}\tag{2.37}$$

REMARK 2.3. In all numerical examples, we use the strong stability third-order Runge-Kutta method [29] to discretize the system (2.1) in time, which reads as follows

$$\begin{aligned}
\mathbf{U}^{(1)} &= \mathbf{U}^{(n)}+\Delta t\mathbf{R}\big(\mathbf{U}^{(n)}\big)\\
\mathbf{U}^{(2)} &= \tfrac{3}{4}\mathbf{U}^{(n)}+\tfrac{1}{4}\big(\mathbf{U}^{(1)}+\Delta t\mathbf{R}\big(\mathbf{U}^{(1)}\big)\big)\\
\mathbf{U}^{(n+1)} &= \tfrac{1}{3}\mathbf{U}^{(n)}+\tfrac{2}{3}\big(\mathbf{U}^{(2)}+\Delta t\mathbf{R}\big(\mathbf{U}^{(2)}\big)\big),
\end{aligned}$$

where $\mathbf{R}(\mathbf{U})$ denotes the residuum given by (2.1).

REMARK 2.4. It is worth noticing that the numerical methods (2.26)-(2.29) are Godunov-type path-conservative schemes defined in [12]. The discretization of the source term can also be interpreted using the subcell reconstruction proposed in [11].

REMARK 2.5. $(h_k)^*_{j+\frac{1}{2}\pm}=(h_k)_{j+\frac{1}{2}\pm}$. It should be pointed out that, in [12], they claimed that the numerical solutions of the path-conservative scheme converge to a nonconservative hyperbolic system with error source term in general sense. The current numerical scheme (2.26)-(2.29) also suffers from this difficulty.

3. Positivity-preserving and well-balancing

In this section, we first prove that the new second-order central scheme can preserve the two-layered heights to be non-negative. Then, we prove that the new scheme is well-balanced for the still water (1.2) even when the computational domain contains wet-dry fronts. We consider two time levels t^n and $t^{n+1} := t^n + \Delta t$, and use the first-order forward Euler method to discretize the system (2.1) in time.

THEOREM 3.1 (positivity preserving). *We consider the Equation (2.1). Assume the system (2.1) is discretized by the first-order forward Euler method in time, if* $(\overline{h}_1)_j^n \geq 0, (\overline{h}_2)_j^n \geq 0$ *for all* $j \in \mathbb{Z}$, *and the CFL condition satisfies:* $\nu\alpha \leq \frac{1}{2}$, *here* $\nu = \frac{\Delta t}{\Delta x}$, *where* α *is taken from (2.16). Then, we obtain* $(\overline{h}_1)_j^{n+1} \geq 0, (\overline{h}_2)_j^{n+1} \geq 0$ *for all* $j \in \mathbb{Z}$.

Proof. We first prove that the current scheme can preserve the layered height $(\overline{h}_1)_j^{n+1}$ to be non-negative. Thanks to Remark 2.1, using the reconstruction (2.6)-(2.7), we obtain

$$0 \leq (h_1)^*_{j+\frac{1}{2}-} \leq (h_1)_{j+\frac{1}{2}-}, \quad 0 \leq (h_1)^*_{j-\frac{1}{2}+} \leq (h_1)_{j-\frac{1}{2}+}.$$

Then cell average of the layered height satisfies,

$$(\overline{h}_1)_j^n = \frac{(h_1)_{j-\frac{1}{2}+} + (h_1)_{j+\frac{1}{2}-}}{2} \geq \frac{(h_1)^*_{j-\frac{1}{2}+} + (h_1)^*_{j+\frac{1}{2}-}}{2}. \tag{3.1}$$

Using the numerical flux (2.15)-(2.16), we first compute,

$$\begin{aligned}
&\mathbf{F}^{(1)}_{j+\frac{1}{2}} - \mathbf{F}^{(1)}_{j-\frac{1}{2}} \\
=&\frac{1}{2}\left[(h_1)^*_{j+\frac{1}{2}+}(u_1)_{j+\frac{1}{2}+} + (h_1)^*_{j+\frac{1}{2}-}(u_1)_{j+\frac{1}{2}-} - \alpha_{j+\frac{1}{2}}\left((h_1)^*_{j+\frac{1}{2}+} - (h_1)^*_{j+\frac{1}{2}-}\right)\right] \\
&-\frac{1}{2}\left[(h_1)^*_{j-\frac{1}{2}+}(u_1)_{j-\frac{1}{2}+} + (h_1)^*_{j-\frac{1}{2}-}(u_1)_{j-\frac{1}{2}-} - \alpha_{j-\frac{1}{2}}\left((h_1)^*_{j-\frac{1}{2}+} - (h_1)^*_{j-\frac{1}{2}-}\right)\right] \\
=&\frac{1}{2}(h_1)^*_{j+\frac{1}{2}+}\left((u_1)_{j+\frac{1}{2}+} - \alpha_{j+\frac{1}{2}}\right) + \frac{1}{2}(h_1)^*_{j+\frac{1}{2}-}\left((u_1)_{j+\frac{1}{2}-} + \alpha_{j+\frac{1}{2}}\right) \\
&-\frac{1}{2}(h_1)^*_{j-\frac{1}{2}+}\left((u_1)_{j-\frac{1}{2}+} - \alpha_{j-\frac{1}{2}}\right) - \frac{1}{2}(h_1)^*_{j-\frac{1}{2}-}\left((u_1)_{j-\frac{1}{2}-} + \alpha_{j-\frac{1}{2}}\right).
\end{aligned} \tag{3.2}$$

According to the first components of Equations (2.1) and (3.2), we obtain:

$$\begin{aligned}
(\overline{h}_1)_j^{n+1} =& (\overline{h}_1)_j^n - \nu\left(\mathbf{F}^{(1)}_{j+\frac{1}{2}} - \mathbf{F}^{(1)}_{j-\frac{1}{2}}\right) \\
=& \frac{(h_1)_{j-\frac{1}{2}+} + (h_1)_{j+\frac{1}{2}-}}{2} - \nu\left(\mathbf{F}^{(1)}_{j+\frac{1}{2}} - \mathbf{F}^{(1)}_{j-\frac{1}{2}}\right) \\
=& \frac{(h_1)_{j-\frac{1}{2}+} + (h_1)_{j+\frac{1}{2}-}}{2} \\
&-\frac{\nu}{2}\left[(h_1)^*_{j+\frac{1}{2}+}\left((u_1)_{j+\frac{1}{2}+} - \alpha_{j+\frac{1}{2}}\right) + (h_1)^*_{j+\frac{1}{2}-}\left((u_1)_{j+\frac{1}{2}-} + \alpha_{j+\frac{1}{2}}\right)\right] \\
&+\frac{\nu}{2}\left[(h_1)^*_{j-\frac{1}{2}+}\left((u_1)_{j-\frac{1}{2}+} - \alpha_{j-\frac{1}{2}}\right) + (h_1)^*_{j-\frac{1}{2}-}\left((u_1)_{j-\frac{1}{2}-} + \alpha_{j-\frac{1}{2}}\right)\right].
\end{aligned}$$

Then, according to (3.1) and the *CFL* condition, the height of $(\overline{h}_1)_j^{n+1}$ satisfies

$$\begin{aligned}
(\overline{h}_1)_j^{n+1} \geq& \left[1 - \nu\left((u_1)_{j+\frac{1}{2}-} + \alpha_{j+\frac{1}{2}}\right)\right]\frac{(h_1)^*_{j+\frac{1}{2}-}}{2} + \left[1 + \nu\left((u_1)_{j-\frac{1}{2}+} - \alpha_{j-\frac{1}{2}}\right)\right]\frac{(h_1)^*_{j-\frac{1}{2}+}}{2} \\
&-\nu\left((u_1)_{j+\frac{1}{2}-} - \alpha_{j+\frac{1}{2}}\right)\frac{(h_1)^*_{j+\frac{1}{2}+}}{2} + \nu\left((u_1)_{j-\frac{1}{2}-} + \alpha_{j-\frac{1}{2}}\right)\frac{(h_1)^*_{j-\frac{1}{2}-}}{2}.
\end{aligned}$$

Since all the coefficients are non-negative in the above inequality, we can obtain $(\overline{h}_1)_j^{n+1} \geq 0$.

The positivity of $(\overline{h}_2)_j^{n+1} \geq 0$ can be obtained by using the analogous method that is used to prove $(\overline{h}_1)_j^{n+1} \geq 0$. We completed the proof. ∎

In the following theorem, we prove that the present scheme is well-balanced for the still water. We should prove four cases: (i) the fully wet case; (ii) only the upper layer has the wet-dry front; (iii) only the lower layer has the wet-dry front; (iv) both the upper and the lower layer have the wet-dry front. In what follows, we suppose the bottom topography satisfies

$$z_{j-\frac{1}{2}-} > z_{j-\frac{1}{2}+} > z_{j+\frac{1}{2}-} > z_{j+\frac{1}{2}+}.$$

We begin with proving the fully wet case.

THEOREM 3.2. *The new second-order central scheme (2.1), (2.7)-(2.10), (2.15) and (2.36) is well-balanced for the still water when the computational domain does not have wet-dry fronts.*

Proof. In this case, the height of the upper layer and the interface are constants, we assume to be h_1 and W respectively. Using the reconstruction (2.6) - (2.7), we can obtain the intermediate bottom level and the intermediate water depth at the cell interface,

$$\begin{aligned}
&z_{j-\frac{1}{2}} = \widehat{z}_{j-\frac{1}{2}} = z_{j-\frac{1}{2}-}, \quad z_{j+\frac{1}{2}} = \widehat{z}_{j+\frac{1}{2}} = z_{j+\frac{1}{2}-},\\
&(h_1)^*_{j-\frac{1}{2}-} = (h_1)^*_{j-\frac{1}{2}+} = h_1, \quad (h_1)^*_{j+\frac{1}{2}-} = (h_1)^*_{j+\frac{1}{2}+} = h_1,\\
&(h_2)^*_{j-\frac{1}{2}-} = (h_2)^*_{j-\frac{1}{2}+} = (h_2)_{j-\frac{1}{2}-}, \quad (h_2)^*_{j+\frac{1}{2}-} = (h_2)^*_{j+\frac{1}{2}+} = (h_2)_{j+\frac{1}{2}-},
\end{aligned} \tag{3.3}$$

and using the Equation (2.8), the modified interface water height is computed by

$$\begin{aligned}
(h_1)_{j-\frac{1}{2}} &= \frac{(h_1)^*_{j-\frac{1}{2}-} + (h_1)^*_{j-\frac{1}{2}+}}{2} = h_1,\\
(h_1)_{j+\frac{1}{2}} &= \frac{(h_1)^*_{j+\frac{1}{2}-} + (h_1)^*_{j+\frac{1}{2}+}}{2} = h_1,\\
(h_2)_{j-\frac{1}{2}} &= \frac{(h_2)^*_{j-\frac{1}{2}-} + (h_2)^*_{j-\frac{1}{2}+}}{2} = (h_2)_{j-\frac{1}{2}-},\\
(h_2)_{j+\frac{1}{2}} &= \frac{(h_2)^*_{j+\frac{1}{2}-} + (h_2)^*_{j+\frac{1}{2}+}}{2} = (h_2)_{j+\frac{1}{2}-}.
\end{aligned} \tag{3.4}$$

Note that since in this case the height of the upper layer is constant, the proof is a direct application of the same property for the classical (single-layer) shallow water system, already demonstrated in [11]. Then, we can prove that $\mathbf{R}_j^{(2)} = 0$.

Next, we prove $\mathbf{R}_j^{(4)} = 0$. Noting that $\widetilde{h}_1 = rh_1$, here r is a constant. Using (3.3) - (3.4) and (2.36), we obtain the discretization of the fourth component of the source term

$$\begin{aligned}
\mathbf{S}^{(4)}_{j-\frac{1}{2}+} &= -\frac{1}{2}g\left((h_2)_{j-\frac{1}{2}+} + (h_2)^*_{j-\frac{1}{2}+}\right)\left(z_{j-\frac{1}{2}+} + (\widetilde{h}_1)^*_{j-\frac{1}{2}+} - \widehat{z}_{j-\frac{1}{2}} - (\widetilde{h}_1)_{j-\frac{1}{2}}\right)\\
&= -\frac{1}{2}g\left((h_2)_{j-\frac{1}{2}+} + (h_2)^*_{j-\frac{1}{2}+}\right)\left(W - (h_2)_{j-\frac{1}{2}+} - W + (h_2)_{j-\frac{1}{2}-}\right)
\end{aligned}$$

$$
\begin{aligned}
&= -\frac{1}{2}g\left((h_2)^2_{j-\frac{1}{2}-} - (h_2)^2_{j-\frac{1}{2}+}\right),\\
\mathbf{S}^{(4)}_{j+\frac{1}{2}-} &= -\frac{1}{2}g\left((h_2)^*_{j+\frac{1}{2}-} + (h_2)_{j+\frac{1}{2}-}\right)\left(\widehat{z}_{j+\frac{1}{2}} + (\widetilde{h}_1)_{j+\frac{1}{2}} - z_{j+\frac{1}{2}-} - (\widetilde{h}_1)^*_{j+\frac{1}{2}-}\right)\\
&= 0\\
\mathbf{S}^{(4)}_{j} &= -\frac{1}{2}g\left((h_2)_{j-\frac{1}{2}+} + (h_2)_{j+\frac{1}{2}-}\right)\left(z_{j+\frac{1}{2}-} + (\widetilde{h}_1)_{j+\frac{1}{2}-} - z_{j-\frac{1}{2}+} - (\widetilde{h}_1)_{j-\frac{1}{2}+}\right), \quad (3.5)\\
&= -\frac{1}{2}g\left((h_2)_{j-\frac{1}{2}+} + (h_2)_{j+\frac{1}{2}-}\right)\left(W - (h_2)_{j+\frac{1}{2}-} - W + (h_2)_{j-\frac{1}{2}+}\right)\\
&= -\frac{1}{2}g\left((h_2)^2_{j-\frac{1}{2}+} - (h_2)^2_{j+\frac{1}{2}-}\right).
\end{aligned}
$$

The fourth component of the numerical fluxes are computed by:

$$
\begin{aligned}
\mathbf{F}^{(4)}_{j+\frac{1}{2}} =& \frac{1}{4}g\left[\left((h_2)^*_{j+\frac{1}{2}+}\right)^2 + \left((h_2)^*_{j+\frac{1}{2}-}\right)^2\right]\\
&- \frac{1}{2}\alpha_{j+\frac{1}{2}}\left((h_2)^*_{j+\frac{1}{2}+}(u_2)_{j+\frac{1}{2}+} - (h_2)^*_{j+\frac{1}{2}-}(u_2)_{j+\frac{1}{2}-}\right)\\
=& \frac{1}{2}g\left((h_2)_{j+\frac{1}{2}-}\right)^2,\\
\mathbf{F}^{(4)}_{j-\frac{1}{2}} =& \frac{1}{4}g\left[\left((h_2)^*_{j-\frac{1}{2}+}\right)^2 + \left((h_2)^*_{j-\frac{1}{2}-}\right)^2\right]\\
&- \frac{1}{2}\alpha_{j-\frac{1}{2}}\left((h_2)^*_{j-\frac{1}{2}+}(u_2)_{j-\frac{1}{2}+} - (h_2)^*_{j-\frac{1}{2}-}(u_2)_{j-\frac{1}{2}-}\right)\\
=& \frac{1}{2}g\left((h_2)_{j-\frac{1}{2}-}\right)^2,
\end{aligned}
$$

then, we obtain

$$
\begin{aligned}
\Delta x\mathbf{R}^{(4)}_j &= \mathbf{F}^{(4)}_{j-\frac{1}{2}} - \mathbf{F}^{(4)}_{j+\frac{1}{2}} + \mathbf{S}^{(4)}_{j-\frac{1}{2}+} + \mathbf{S}^{(4)}_{j} + \mathbf{S}^{(4)}_{j+\frac{1}{2}-}\\
&= \frac{1}{2}g\left(\left((h_2)_{j-\frac{1}{2}-}\right)^2 - \left((h_2)_{j+\frac{1}{2}-}\right)^2\right) - \frac{1}{2}g\left(\left((h_2)_{j-\frac{1}{2}-}\right)^2 - \left((h_2)_{j+\frac{1}{2}-}\right)^2\right)\\
&= 0.
\end{aligned}
$$

□

The following theorem proves the well-balanced property of the current scheme for the system with wet-dry fronts.

THEOREM 3.3. *The new second-order central scheme (2.1), (2.7)-(2.10), (2.15) and (2.36) is well-balanced for the still water when the computational domain has wet-dry fronts.*

Proof. In this case, we should consider three cases: (A1) only the upper layer has the wet-dry front; (A2) only the lower layer has the wet-dry front; (A3) both the upper and the lower layer have the wet-dry front. We begin with only the upper layer having the wet-dry front.

• *Case* (A1) Only the upper layer has the wet-dry front, as shown in the middle part of the Figure 3.1. In this case, the system (1.1) changes to be the classical one-layer shallow water equations. The well-balanced property is similar to that in [11], because the reconstruction (2.7) is the *subcell reconstructions* proposed in [11]. Then, we omit the details.

• *Case* (A2) Only the lower layer has the wet-dry front, as shown in the left part of the Figure 3.1. In this case, the total level is a constant, we assume is E. Using

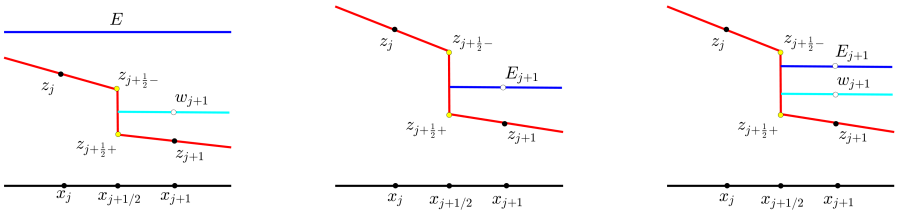

FIG. 3.1. *Three partially-wet cases. Left: only the lower layer has wet-dry front; Middle: only the upper layer has wet-dry front; Right: Both the layers have wet-dry front.*

the reconstruction (2.6) - (2.7), we can obtain the intermediate bottom level and the intermediate water depth at the cell interface,

$$\begin{aligned}
&z_{j-\frac{1}{2}} = z_{j-\frac{1}{2}-}, \quad z_{j+\frac{1}{2}} = z_{j+\frac{1}{2}-},\\
&\widehat{z}_{j-\frac{1}{2}} = w_{j-\frac{1}{2}+}, \quad \widehat{z}_{j+\frac{1}{2}} = z_{j+\frac{1}{2}-},\\
&(h_1)^*_{j-\frac{1}{2}-} = (h_1)^*_{j-\frac{1}{2}+} = (h_1)_{j-\frac{1}{2}-}, \quad (h_1)^*_{j+\frac{1}{2}-} = (h_1)^*_{j+\frac{1}{2}+} = (h_1)_{j+\frac{1}{2}-},\\
&(h_2)^*_{j-\frac{1}{2}-} = (h_2)^*_{j-\frac{1}{2}+} = 0, \quad (h_2)^*_{j+\frac{1}{2}-} = (h_2)^*_{j+\frac{1}{2}+} = (h_2)_{j+\frac{1}{2}-},
\end{aligned} \tag{3.6}$$

and using the Equation (2.8), the modified interface water height is computed by

$$\begin{aligned}
(h_1)_{j-\frac{1}{2}} &= \frac{(h_1)^*_{j-\frac{1}{2}-} + (h_1)^*_{j-\frac{1}{2}+}}{2} = (h_1)_{j-\frac{1}{2}-},\\
(h_1)_{j+\frac{1}{2}} &= \frac{(h_1)^*_{j+\frac{1}{2}-} + (h_1)^*_{j+\frac{1}{2}+}}{2} = (h_1)_{j+\frac{1}{2}-},\\
(h_2)_{j-\frac{1}{2}} &= \frac{(h_2)^*_{j-\frac{1}{2}-} + (h_2)^*_{j-\frac{1}{2}+}}{2} = 0,\\
(h_2)_{j+\frac{1}{2}} &= \frac{(h_2)^*_{j+\frac{1}{2}-} + (h_2)^*_{j+\frac{1}{2}+}}{2} = (h_2)_{j+\frac{1}{2}-}.
\end{aligned} \tag{3.7}$$

Then, we first prove $\mathbf{R}^{(2)}_j = 0$. Using (3.6) - (3.7) and (2.36), we obtain the discretization of the second component of the source term

$$\begin{aligned}
\mathbf{S}^{(2)}_{j-\frac{1}{2}+} &= -\frac{1}{2}g\left((h_1)_{j-\frac{1}{2}+} + (h_1)^*_{j-\frac{1}{2}+}\right)\left(z_{j-\frac{1}{2}+} + (h_2)_{j-\frac{1}{2}+} - z_{j-\frac{1}{2}} - (h_2)_{j-\frac{1}{2}}\right)\\
&= -\frac{1}{2}g\left((h_1)_{j-\frac{1}{2}+} + (h_1)^*_{j-\frac{1}{2}+}\right)\left(w_{j-\frac{1}{2}+} - z_{j-\frac{1}{2}}\right)\\
&= -\frac{1}{2}g\left((h_1)_{j-\frac{1}{2}+} + (h_1)^*_{j-\frac{1}{2}+}\right)\left(E - (h_1)_{j-\frac{1}{2}+} - E + (h_1)_{j-\frac{1}{2}-}\right)\\
&= -\frac{1}{2}g\left(\left((h_1)_{j-\frac{1}{2}-}\right)^2 - \left((h_1)_{j-\frac{1}{2}+}\right)^2\right),\\
\mathbf{S}^{(2)}_{j+\frac{1}{2}-} &= -\frac{1}{2}g\left((h_1)^*_{j+\frac{1}{2}-} + (h_1)_{j+\frac{1}{2}-}\right)\left(z_{j+\frac{1}{2}} + (h_2)_{j+\frac{1}{2}} - z_{j+\frac{1}{2}-} - (h_2)_{j+\frac{1}{2}-}\right)\\
&= 0,\\
\mathbf{S}^{(2)}_{j} &= -\frac{1}{2}g\left((h_1)_{j-\frac{1}{2}+} + (h_1)_{j+\frac{1}{2}-}\right)\left(z_{j+\frac{1}{2}-} + (h_2)_{j+\frac{1}{2}-} - z_{j-\frac{1}{2}+} - (h_2)_{j-\frac{1}{2}+}\right)\\
&= 0.
\end{aligned}$$

The second component of the numerical fluxes are computed by:

$$\begin{aligned}\mathbf{F}^{(2)}_{j+\frac{1}{2}} =& \frac{1}{4}g\left[\left((h_1)^*_{j+\frac{1}{2}+}\right)^2+\left((h_1)^*_{j+\frac{1}{2}-}\right)^2\right]\\ &-\frac{1}{2}\alpha_{j+\frac{1}{2}}\left((h_1)^*_{j+\frac{1}{2}+}(u_1)_{j+\frac{1}{2}+}-(h_1)^*_{j+\frac{1}{2}-}(u_1)_{j+\frac{1}{2}-}\right)\\ =&\frac{1}{2}g\left((h_1)_{j+\frac{1}{2}-}\right)^2=\frac{1}{2}g\left((h_1)_{j-\frac{1}{2}+}\right)^2\\ \mathbf{F}^{(2)}_{j-\frac{1}{2}} =& \frac{1}{4}g\left[\left((h_1)^*_{j-\frac{1}{2}+}\right)^2+\left((h_1)^*_{j-\frac{1}{2}-}\right)^2\right]\\ &-\frac{1}{2}\alpha_{j-\frac{1}{2}}\left((h_1)^*_{j-\frac{1}{2}+}(u_1)_{j-\frac{1}{2}+}-(h_1)^*_{j-\frac{1}{2}-}(u_1)_{j-\frac{1}{2}-}\right)\\ =&\frac{1}{2}g\left((h_1)_{j-\frac{1}{2}-}\right)^2,\end{aligned}$$

then, a straightforward calculation gives

$$\begin{aligned}\Delta x\mathbf{R}^{(2)}_j =& \mathbf{F}^{(2)}_{j-\frac{1}{2}}-\mathbf{F}^{(2)}_{j+\frac{1}{2}}+\mathbf{S}^{(2)}_{j-\frac{1}{2}+}+\mathbf{S}^{(2)}_j+\mathbf{S}^{(2)}_{j+\frac{1}{2}-}\\ =&-\frac{1}{2}g\left((h_1)_{j-\frac{1}{2}+}\right)^2+\frac{1}{2}g\left((h_1)_{j-\frac{1}{2}-}\right)^2-\frac{1}{2}g\left(\left((h_1)_{j-\frac{1}{2}-}\right)^2-\left((h_1)_{j-\frac{1}{2}+}\right)^2\right)\\ =&0.\end{aligned}$$

Next, we prove $\mathbf{R}^{(4)}_j=0$. Noting that $\widetilde{h}_1=rh_1$, here r is a constant. Using (3.6) - (3.7) and (2.36), we obtain the discretization of the fourth component of the source term

$$\begin{aligned}\mathbf{S}^{(4)}_{j-\frac{1}{2}+} =& -\tfrac{1}{2}g\left((h_2)_{j-\frac{1}{2}+}+(h_2)^*_{j-\frac{1}{2}+}\right)\left(z_{j-\frac{1}{2}+}+(\widetilde{h}_1)^*_{j-\frac{1}{2}+}-\widehat{z}_{j-\frac{1}{2}}-(\widetilde{h}_1)_{j-\frac{1}{2}}\right)\\ =&-\tfrac{1}{2}g\left((h_2)_{j-\frac{1}{2}+}\right)\left(z_{j-\frac{1}{2}+}-w_{j-\frac{1}{2}+}\right)\\ =&\tfrac{1}{2}g\left((h_2)_{j-\frac{1}{2}+}\right)^2,\\ \mathbf{S}^{(4)}_{j+\frac{1}{2}-} =& -\tfrac{1}{2}g\left((h_2)^*_{j+\frac{1}{2}-}+(h_2)_{j+\frac{1}{2}-}\right)\left(\widehat{z}_{j+\frac{1}{2}}+(\widetilde{h}_1)_{j+\frac{1}{2}}-z_{j+\frac{1}{2}-}-(\widetilde{h}_1)^*_{j+\frac{1}{2}-}\right)\\ =&0,\\ \mathbf{S}^{(4)}_j =& -\tfrac{1}{2}g\left((h_2)_{j-\frac{1}{2}+}+(h_2)_{j+\frac{1}{2}-}\right)\left(z_{j+\frac{1}{2}-}+(\widetilde{h}_1)_{j+\frac{1}{2}-}-z_{j-\frac{1}{2}+}-(\widetilde{h}_1)_{j-\frac{1}{2}+}\right)\\ =&-\tfrac{1}{2}g\left((h_2)_{j-\frac{1}{2}+}+(h_2)_{j+\frac{1}{2}-}\right)\left(w_{j+\frac{1}{2}-}-(h_2)_{j+\frac{1}{2}-}-w_{j-\frac{1}{2}+}+(h_2)_{j-\frac{1}{2}+}\right)\\ =&-\tfrac{1}{2}g\left((h_2)^2_{j-\frac{1}{2}+}-(h_2)^2_{j+\frac{1}{2}-}\right).\end{aligned}\tag{3.8}$$

The fourth component of the numerical fluxes are computed by:

$$\begin{aligned}\mathbf{F}^{(4)}_{j+\frac{1}{2}} =& \frac{1}{4}g\left[\left((h_2)^*_{j+\frac{1}{2}+}\right)^2+\left((h_2)^*_{j+\frac{1}{2}-}\right)^2\right]\\ &-\frac{1}{2}\alpha_{j+\frac{1}{2}}\left((h_2)^*_{j+\frac{1}{2}+}(u_2)_{j+\frac{1}{2}+}-(h_2)^*_{j+\frac{1}{2}-}(u_2)_{j+\frac{1}{2}-}\right)\\ =&\frac{1}{2}g\left((h_2)_{j+\frac{1}{2}-}\right)^2,\\ \mathbf{F}^{(4)}_{j-\frac{1}{2}} =& \frac{1}{4}g\left[\left((h_2)^*_{j-\frac{1}{2}+}\right)^2+\left((h_2)^*_{j-\frac{1}{2}-}\right)^2\right]\\ &-\frac{1}{2}\alpha_{j-\frac{1}{2}}\left((h_2)^*_{j-\frac{1}{2}+}(u_2)_{j-\frac{1}{2}+}-(h_2)^*_{j-\frac{1}{2}-}(u_2)_{j-\frac{1}{2}-}\right)\\ =&0,\end{aligned}$$

then, we obtain

$$\begin{aligned}\Delta x\mathbf{R}_j^{(4)} &= \mathbf{F}_{j-\frac{1}{2}}^{(4)} - \mathbf{F}_{j+\frac{1}{2}}^{(4)} + \mathbf{S}_{j-\frac{1}{2}+}^{(4)} + \mathbf{S}_j^{(4)} + \mathbf{S}_{j+\frac{1}{2}-}^{(4)} \\ &= -\frac{1}{2}g\left((h_2)_{j+\frac{1}{2}-}\right)^2 + \frac{1}{2}g\left((h_2)_{j-\frac{1}{2}+}\right)^2 - \frac{1}{2}g\left(\left((h_2)_{j-\frac{1}{2}+}\right)^2 - \left((h_2)_{j+\frac{1}{2}-}\right)^2\right) \\ &= 0.\end{aligned}$$

It remains to prove the final case: (A3).

• *Case* (A3) Both the upper and the lower layers have the wet-dry front, as shown in the right part of the Figure 3.1. Using the reconstruction (2.6) - (2.7), we can obtain the intermediate bottom level and the intermediate water depth at the cell interface,

$$\begin{aligned}&z_{j-\frac{1}{2}} = E_{j-\frac{1}{2}-}, \quad z_{j+\frac{1}{2}} = z_{j+\frac{1}{2}-}, \\ &\widehat{z}_{j-\frac{1}{2}} = w_{j-\frac{1}{2}+}, \quad \widehat{z}_{j+\frac{1}{2}} = z_{j+\frac{1}{2}-}, \\ &(h_1)^*_{j-\frac{1}{2}-} = (h_1)^*_{j-\frac{1}{2}+} = 0, \quad (h_1)^*_{j+\frac{1}{2}-} = (h_1)^*_{j+\frac{1}{2}+} = (h_1)_{j+\frac{1}{2}-}, \\ &(h_2)^*_{j-\frac{1}{2}-} = (h_2)^*_{j-\frac{1}{2}+} = 0, \quad (h_2)^*_{j+\frac{1}{2}-} = (h_2)^*_{j+\frac{1}{2}+} = (h_2)_{j+\frac{1}{2}-},\end{aligned} \tag{3.9}$$

and using the Equation (2.8), the modified interface water height is computed by

$$\begin{aligned}(h_1)_{j-\frac{1}{2}} &= \frac{(h_1)^*_{j-\frac{1}{2}-} + (h_1)^*_{j-\frac{1}{2}+}}{2} = 0, \; (h_1)_{j+\frac{1}{2}} = \frac{(h_1)^*_{j+\frac{1}{2}-} + (h_1)^*_{j+\frac{1}{2}+}}{2} = (h_1)_{j+\frac{1}{2}-}, \\ (h_2)_{j-\frac{1}{2}} &= \frac{(h_2)^*_{j-\frac{1}{2}-} + (h_2)^*_{j-\frac{1}{2}+}}{2} = 0, \; (h_2)_{j+\frac{1}{2}} = \frac{(h_2)^*_{j+\frac{1}{2}-} + (h_2)^*_{j+\frac{1}{2}+}}{2} = (h_2)_{j+\frac{1}{2}-}.\end{aligned} \tag{3.10}$$

Then, we first prove $\mathbf{R}_j^{(2)} = 0$. Using (3.9) - (3.10) and (2.36), we obtain the discretization of the second component of the source term

$$\begin{aligned}\mathbf{S}_{j-\frac{1}{2}+}^{(2)} &= -\tfrac{1}{2}g\left((h_1)_{j-\frac{1}{2}+} + (h_1)^*_{j-\frac{1}{2}+}\right)\left(z_{j-\frac{1}{2}+} + (h_2)_{j-\frac{1}{2}+} - z_{j-\frac{1}{2}} - (h_2)_{j-\frac{1}{2}}\right), \\ &= -\tfrac{1}{2}g\left((h_1)_{j-\frac{1}{2}+} + (h_1)^*_{j-\frac{1}{2}+}\right)\left(w_{j-\frac{1}{2}+} - E_{j-\frac{1}{2}+}\right) \\ &= \tfrac{1}{2}g\left((h_1)_{j-\frac{1}{2}+}\right)^2, \\ \mathbf{S}_{j+\frac{1}{2}-}^{(2)} &= -\tfrac{1}{2}g\left((h_1)^*_{j+\frac{1}{2}-} + (h_1)_{j+\frac{1}{2}-}\right)\left(z_{j+\frac{1}{2}} + (h_2)_{j+\frac{1}{2}} - z_{j+\frac{1}{2}-} - (h_2)_{j+\frac{1}{2}-}\right), \\ &= 0, \\ \mathbf{S}_j^{(2)} &= -\tfrac{1}{2}g\left((h_1)_{j-\frac{1}{2}+} + (h_1)_{j+\frac{1}{2}-}\right)\left(z_{j+\frac{1}{2}-} + (h_2)_{j+\frac{1}{2}-} - z_{j-\frac{1}{2}+} - (h_2)_{j-\frac{1}{2}+}\right), \\ &= 0.\end{aligned}$$

The second component of the numerical fluxes are computed by:

$$\begin{aligned}\mathbf{F}_{j+\frac{1}{2}}^{(2)} &= \frac{1}{4}g\left[\left((h_1)^*_{j+\frac{1}{2}+}\right)^2 + \left((h_1)^*_{j+\frac{1}{2}-}\right)^2\right] \\ &\quad - \frac{1}{2}\alpha_{j+\frac{1}{2}}\left((h_1)^*_{j+\frac{1}{2}+}(u_1)_{j+\frac{1}{2}+} - (h_1)^*_{j+\frac{1}{2}-}(u_1)_{j+\frac{1}{2}-}\right) \\ &= \frac{1}{2}g\left((h_1)_{j+\frac{1}{2}-}\right)^2 = \frac{1}{2}g\left((h_1)_{j-\frac{1}{2}+}\right)^2, \\ \mathbf{F}_{j-\frac{1}{2}}^{(2)} &= \frac{1}{4}g\left[\left((h_1)^*_{j-\frac{1}{2}+}\right)^2 + \left((h_1)^*_{j-\frac{1}{2}-}\right)^2\right] \\ &\quad - \frac{1}{2}\alpha_{j-\frac{1}{2}}\left((h_1)^*_{j-\frac{1}{2}+}(u_1)_{j-\frac{1}{2}+} - (h_1)^*_{j-\frac{1}{2}-}(u_1)_{j-\frac{1}{2}-}\right) \\ &= 0,\end{aligned}$$

then, a straightforward calculation gives

$$\begin{aligned}\Delta x\mathbf{R}_j^{(2)} &= \mathbf{F}_{j-\frac{1}{2}}^{(2)} - \mathbf{F}_{j+\frac{1}{2}}^{(2)} + \mathbf{S}_{j-\frac{1}{2}+}^{(2)} + \mathbf{S}_j^{(2)} + \mathbf{S}_{j+\frac{1}{2}-}^{(2)} \\ &= -\frac{1}{2}g\left((h_1)_{j-\frac{1}{2}+}\right)^2 + \frac{1}{2}g\left((h_1)_{j-\frac{1}{2}+}\right)^2 \\ &= 0.\end{aligned}$$

Finally, we prove $\mathbf{R}_j^{(4)} = 0$. Noting that $\widetilde{h}_1 = rh_1$, here r is a constant. Using (3.9) - (3.10) and (2.36), we obtain the discretization of the fourth component of the source term

$$\begin{aligned}\mathbf{S}_{j-\frac{1}{2}+}^{(4)} &= -\frac{1}{2}g\left((h_2)_{j-\frac{1}{2}+} + (h_2)^*_{j-\frac{1}{2}+}\right)\left(z_{j-\frac{1}{2}+} + (\widetilde{h}_1)^*_{j-\frac{1}{2}+} - \widehat{z}_{j-\frac{1}{2}} - (\widetilde{h}_1)_{j-\frac{1}{2}}\right) \\ &= -\frac{1}{2}g\left((h_2)_{j-\frac{1}{2}+}\right)\left(z_{j-\frac{1}{2}+} - w_{j-\frac{1}{2}+}\right) \\ &= \frac{1}{2}g\left((h_2)_{j-\frac{1}{2}+}\right)^2, \\ \mathbf{S}_{j+\frac{1}{2}-}^{(4)} &= -\frac{1}{2}g\left((h_2)^*_{j+\frac{1}{2}-} + (h_2)_{j+\frac{1}{2}-}\right)\left(\widehat{z}_{j+\frac{1}{2}} + (\widetilde{h}_1)_{j+\frac{1}{2}} - z_{j+\frac{1}{2}-} - (\widetilde{h}_1)^*_{j+\frac{1}{2}-}\right) \\ &= 0, \\ \mathbf{S}_j^{(4)} &= -\frac{1}{2}g\left((h_2)_{j-\frac{1}{2}+} + (h_2)_{j+\frac{1}{2}-}\right)\left(z_{j+\frac{1}{2}-} + (\widetilde{h}_1)_{j+\frac{1}{2}-} - z_{j-\frac{1}{2}+} - (\widetilde{h}_1)_{j-\frac{1}{2}+}\right) \\ &= -\frac{1}{2}g\left((h_2)_{j-\frac{1}{2}+} + (h_2)_{j+\frac{1}{2}-}\right)\left(w_{j+\frac{1}{2}-} - (h_2)_{j+\frac{1}{2}-} - w_{j-\frac{1}{2}+} + (h_2)_{j-\frac{1}{2}+}\right) \\ &= -\frac{1}{2}g\left((h_2)^2_{j-\frac{1}{2}+} - (h_2)^2_{j+\frac{1}{2}-}\right). \end{aligned} \tag{3.11}$$

The fourth component of the numerical fluxes are computed by:

$$\begin{aligned}\mathbf{F}_{j+\frac{1}{2}}^{(4)} &= \frac{1}{4}g\left[\left((h_2)^*_{j+\frac{1}{2}+}\right)^2 + \left((h_2)^*_{j+\frac{1}{2}-}\right)^2\right] \\ &\quad - \frac{1}{2}\alpha_{j+\frac{1}{2}}\left((h_2)^*_{j+\frac{1}{2}+}(u_2)_{j+\frac{1}{2}+} - (h_2)^*_{j+\frac{1}{2}-}(u_2)_{j+\frac{1}{2}-}\right) \\ &= \frac{1}{2}g\left((h_2)_{j+\frac{1}{2}-}\right)^2, \\ \mathbf{F}_{j-\frac{1}{2}}^{(4)} &= \frac{1}{4}g\left[\left((h_2)^*_{j-\frac{1}{2}+}\right)^2 + \left((h_2)^*_{j-\frac{1}{2}-}\right)^2\right] \\ &\quad - \frac{1}{2}\alpha_{j-\frac{1}{2}}\left((h_2)^*_{j-\frac{1}{2}+}(u_2)_{j-\frac{1}{2}+} - (h_2)^*_{j-\frac{1}{2}-}(u_2)_{j-\frac{1}{2}-}\right) \\ &= 0,\end{aligned}$$

then, we obtain

$$\begin{aligned}\Delta x\mathbf{R}_j^{(4)} &= \mathbf{F}_{j-\frac{1}{2}}^{(4)} - \mathbf{F}_{j+\frac{1}{2}}^{(2)} + \mathbf{S}_{j-\frac{1}{2}+}^{(4)} + \mathbf{S}_j^{(4)} + \mathbf{S}_{j+\frac{1}{2}-}^{(4)} \\ &= -\frac{1}{2}g\left((h_2)_{j+\frac{1}{2}-}\right)^2 + \frac{1}{2}g\left((h_2)_{j-\frac{1}{2}+}\right)^2 - \frac{1}{2}g\left(\left((h_2)_{j-\frac{1}{2}+}\right)^2 - \left((h_2)_{j+\frac{1}{2}-}\right)^2\right) \\ &= 0.\end{aligned}$$

The proof is completed. ∎

4. Numerical experiments

In this section, we present several computational results of the current scheme for the two-layer shallow water equations with wetting and frying transitions. We set the gravitational acceleration constant to be $g=9.8$ and the CFL number to be 0.4 in all our numerical examples. Let us remark that $ref.\bullet$ denotes the reference solution of $\bullet$.

We first test the numerical order of accuracy of the current scheme. The bottom topography is defined by the following function:

$$z(x)=\sin^2(\pi x),$$

with the initial layered heights and the discharge

$$h_1(x,0)=5+e^{\cos(2\pi x)},\quad h_1u_1(x,0)=h_2u_2(x,0)=0,\quad h_2(x,0)=5-e^{\cos(2\pi x)}.$$

The reference solution is computed by the current scheme with 6400 uniform cells on the computational domain [0, 1]. The final time is $t=0.1$. At this time, the solution is smooth. Table 4.1 shows that our new scheme has second-order accuracy.

Number of the cells	h_1-upper layer height		h_2-lower layer height	
	L_1-**error**	**EOC**	L_1-**error**	**EOC**
100	1.18e-01	-	6.97e-02	-
200	3.95e-02	1.59	2.94e-02	1.25
400	9.90e-03	1.99	7.70e-03	1.94
800	2.50e-03	2.01	1.80e-03	2.07

TABLE 4.1. *Experimental order of convergence (EOC) measured in L_1 - norm.*

4.1. Well-balanced test. In this example, we test the well-balanced property of the current scheme for the still water when the computational domain has wet-dry fronts. We consider two cases: (i) The bottom topography is smooth; (ii) The bottom topography is discontinuous.

For the first case (i): the bottom topography is defined by the following function

$$z(x)=\frac{1}{4}(1-\cos(\pi(2x-1))),\tag{4.1}$$

and the initial data are

$$E(x,0)=\max(0.4,z(x)),\ h_2(x,0)=\max(0.35-z(x),0),\ u_1(x)=u_2(x,0)=0.\tag{4.2}$$

For the second case (ii): the bottom topography is defined by the following function, which is discontinuous at the point $x=0.3$ and $x=0.7$

$$z(x)=\begin{cases}0, & \text{if } 0.3<x<0.7\\ 1, & \text{otherwise.}\end{cases},$$

and the initial data are

$$h_1(x,0)=\begin{cases}0.1, & \text{if } 0.3<x<0.7\\ 0, & \text{otherwise.}\end{cases},h_2(x,0)=\begin{cases}0.4, & \text{if } 0.3<x<0.7\\ 0, & \text{otherwise.}\end{cases},$$
$$u_1(x,0)=u_2(x,0)=0.$$

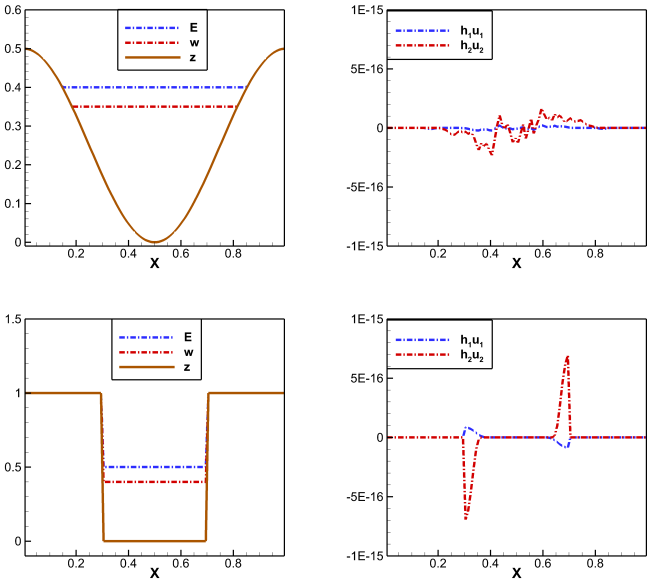

FIG. 4.1. *Well-balanced test. Top Left: the total water height E, the interface w, and the bottom topography B; Top Right: the discharge of two layers corresponds to the smooth bottom topography; Bottom Left: the total water height E, the interface w, and the bottom topography B; Bottom Right: the discharge of two layers corresponds to the discontinuous bottom topography.*

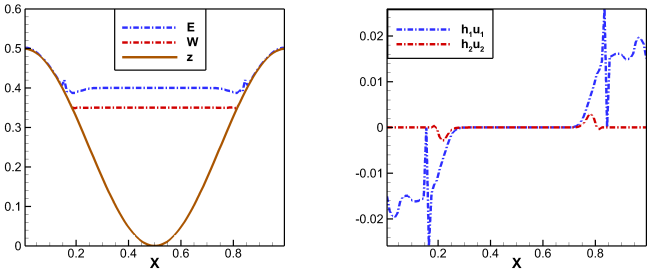

FIG. 4.2. *Well-balanced test. Numerical results obtained by the CU scheme.*

The density ratio is $r = 0.7$. We compute the numerical solution using 100 uniform cells which discretize the computational domain [0, 1]. The final time is $t = 0.5$. In the Figure 4.1, we can observe that the numerical discharge computed by the current scheme is zero (within the machine accuracy) in two cases. These confirm that the current scheme is well-balanced for the still water even when the computational domain has wet-dry fronts.

Finally, we test the well-balanced property of the central-upwind (CU) scheme proposed in [18] using the condition (4.1)-(4.2) to verify the advantage of the present scheme. We show the numerical results obtained by the CU scheme with 100 uniform cells and t = 0.05 in Figure 4.2. One can see spurious oscillations near the wet-dry fronts, which confirm that the CU scheme is not well-balanced when the computational domain contains wet-dry fronts.

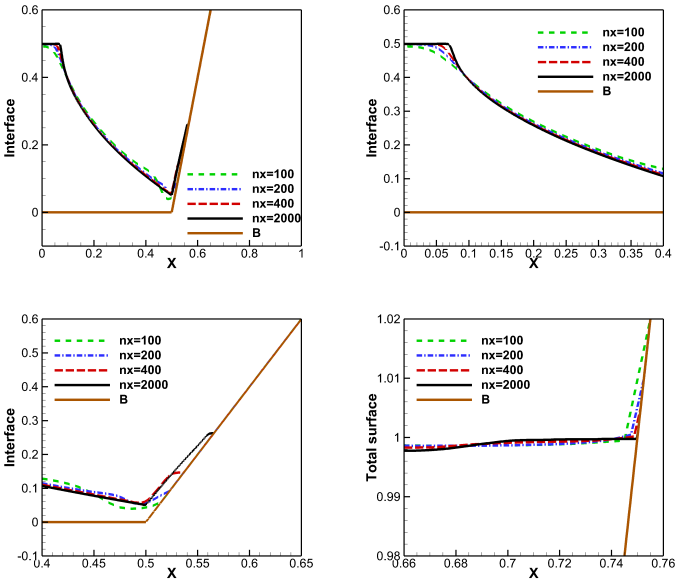

FIG. 4.3. *Topography and drying. Top left: The computed interface using different uniform cells; Top right: A zoom of the interface at interval [0, 0.4]; Bottom left: A zoom of the interface at interval [0.4, 0.65]; Bottom right: A zoom of the total surface at interval [0.66, 0.76].*

4.2. Topography and drying. This test case was proposed in [20]. The constant density ratio is $r=0.95$ and the gravitational constant is $g=9.8$. The bottom topography is given by

$$z(x)=\begin{cases}0, & \text{if } x<0.5,\\ 4(x-0.5), & \text{otherwise,}\end{cases}$$

and the initial data

$$h_2=\begin{cases}0.5, & \text{if } x<0.25\\ 0, & \text{otherwise.}\end{cases}, \qquad h_1=\max(1-h_2-z(x),0),\ u_1=0,\ u_2=0.$$

The computational domain is [0, 1]. The final time is $t=0.5$. The numerical solutions are obtained by the current scheme using different uniform cells: 100, 200, 400, 2000. One can see the computational results in Figure 4.3. The current scheme can guarantee the layered heights to be nonnegative. The numerical results confirm that the current scheme can converge to the reference solutions.

4.3. Small perturbation of the still water over a discontinuous bed. In this example, we consider a small perturbation of the still water steady state solution. The bottom topography has two discontinuities (x = 0.7 and x = 0.8). The computational domain is [0, 1]. The constant density ratio is $r=0.98$ and the gravitational constant is $g=9.8$. The bottom topography is given by

$$z(x)=\begin{cases}1, & \text{if } 0.7<x<0.8,\\ 0, & \text{otherwise,}\end{cases}$$

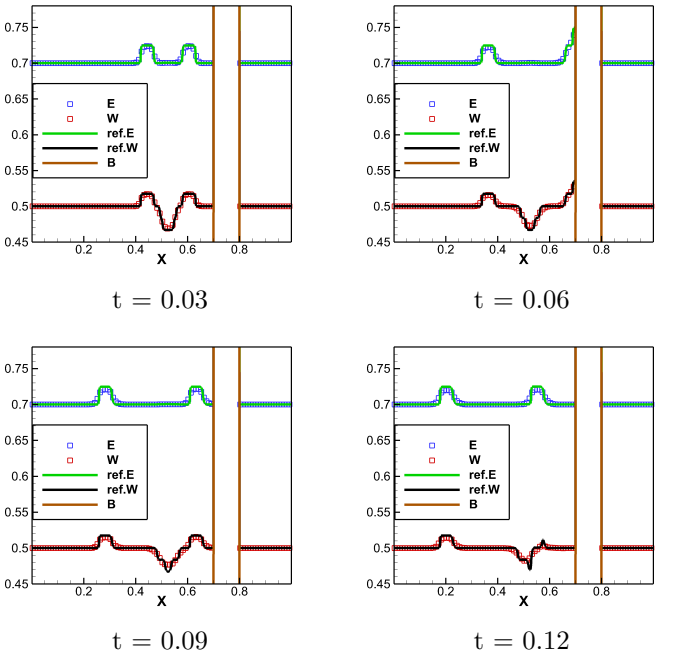

FIG. 4.4. *Small perturbation of the still water over a discontinuous bed. Numerical results of the interface (W) and the total surface (E).*

and the initial data

$$h_1 = \begin{cases} \max(0.7, z(x)) - \max(0.5, z(x)) + 0.05, & \text{if } 0.5 < x < 0.55, \\ \max(0.7, z(x)) - \max(0.5, z(x)), & \text{otherwise.} \end{cases}$$

$$h_2 = \max(0.5 - z(x), 0),\ u_1 = 0,\ u_2 = 0.$$

The output time is $t = 0.03, 0.06, 0.09, 0.12$. We discretize the computational domain using 200 uniform cells. The reference solution is obtained by the current scheme using 2000 uniform cells. The computational results are shown in Figure 4.4. The current scheme can guarantee the layered heights to be nonnegative. The numerical results confirm that the current scheme can capture the small perturbation nicely and avoid producing spurious oscillation near wet-dry fronts.

4.4. Internal dam break over a nonflat bottom. This test problem was also considered in [18]. In this example, the solution of the problem is expected to converge to a steady-state after a long time. The steady state contains a hydraulic jump. It is a challenging task to approximate the hydraulic jump. The computational domain is [-5, 5] and is discretized by 500 uniform cells. The bottom is continuous and is defined by the following function

$$z(x) = 0.5e^{-x^2} - 2.5,$$

and the initial data are

$$(h_1, h_1u_1, h_2, h_2u_2) = \begin{cases} (1.95, 0, -1.95 - B(x), 0), & \text{if } x < 0.0 \\ (0.05, 0, -0.05 - B(x), 0), & \text{otherwise.} \end{cases}$$

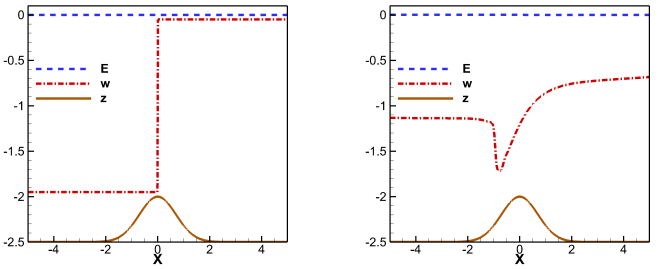

FIG. 4.5. *Internal dam break over a nonflat bottom. Left: the initial time $t=0$; right: the final time $t=200$.*

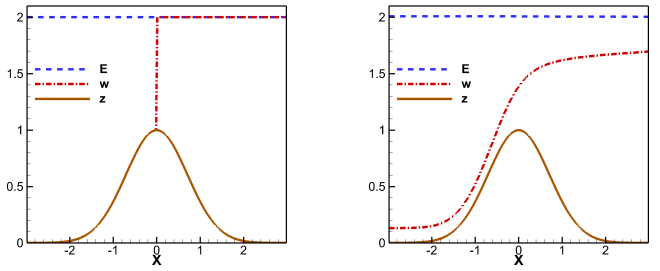

FIG. 4.6. *Lock exchange problem. Left: the initial time $t=0$; right: the final time $t=40$.*

The density ratio is $r=0.998$. We run this simulation until the time $t=200$. The obtained results are shown in Figure 4.5. One can see a high overall resolution of the interface. The numerical results agree well with that obtained in [18].

4.5. Lock exchange problem. This test problem was also discussed in [18]. In this example, we modify the initial data proposed in [18]. Noting that the numerical scheme introduced in [18] is restricted to the amplitude of the total water height, in which the scheme maybe produce spurious oscillations for the large water total height due to the influence of nonconservative product term. The bottom is given by

$$z(x)=e^{-x^2},$$

and the initial data are

$$(h_1,h_1u_1,h_2,h_2u_2)=\begin{cases}(2-B(x),0,0,0), & \text{if } x<0.0,\\ (0,0,2-B(x),0), & \text{otherwise.}\end{cases}$$

The density ratio is $r=0.98$. The boundaries $h_1u_1=-h_2u_2$ are imposed at each end of the computational domain. We compute the numerical solution using 200 uniform cells until $t=40$, which were shown in the Figure 4.6. The numerical results obtained by the current scheme agree well with that of [18] and are similar to the rigid lid approximation proposed in [17]. We can not observe the spurious oscillations. These also confirm that the current scheme is positivity preserving.

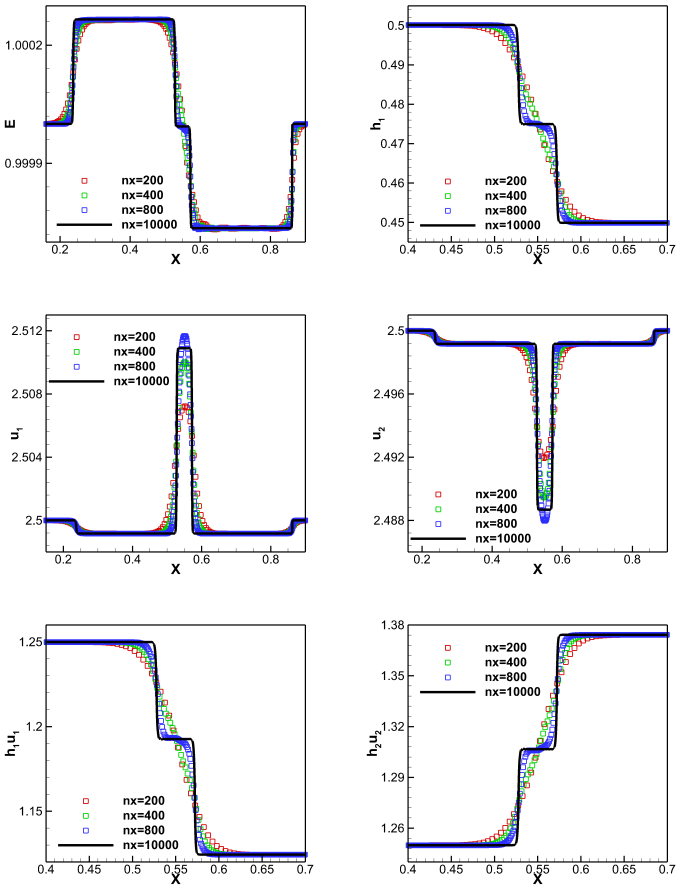

FIG. 4.7. *Interface propagation. Top Left: the total water height E; Top Right: the height of the upper layer h_1; Middle left: the velocity of the upper layer u_1; Middle right: the velocity of the lower layer u_2; Bottom Left: the discharge of the upper layer h_1u_1; Bottom Right: the discharge of the lower layer h_2u_2*

4.6. 1-D Interface propagation. This test problem was also considered in [18]. This example was used to verify that the current scheme is stable. We made a small modification on the initial data. The constant density ratio is $r=0.98$ and the gravitational constant is $g=10$. The bottom topography is $B(x)=0$ and the initial data

$$(h_1,h_1u_1,h_2,h_2u_2)=\begin{cases}(0.50,1.250,0.50,1.250), & \text{if } x<0.3\\ (0.45,1.125,0.55,1.375), & \text{otherwise.}\end{cases}$$

The computational domain is [0,1]. The final time is $t=0.1$. The numerical results are computed by four different uniform meshes: 200, 400, 800, 10^4 uniform cells. One can see the computational results in Figure 4.7. Due to the numerical viscosity, a low resolution and "ENO-type" oscillations can be observed using the coarse mesh. When the grid is refined, one can see a higher resolution and an intermediate state emerges.

Next, we set the bottom topography to be $B(x)=-1$. We compare the numerical results obtained by the new scheme and the CU scheme using 800 uniform cells with

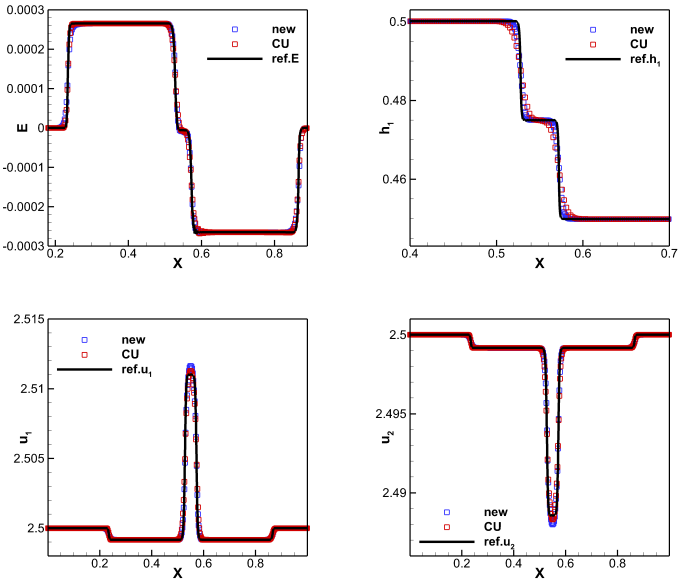

FIG. 4.8. *Interface propagation. Numerical results obtained by the CU scheme. Top Left: the total water height E; Top Right: the height of the upper layer h_1; Bottom Left: the velocity of the upper layer u_1; Bottom Right: the velocity of the lower layer u_2.*

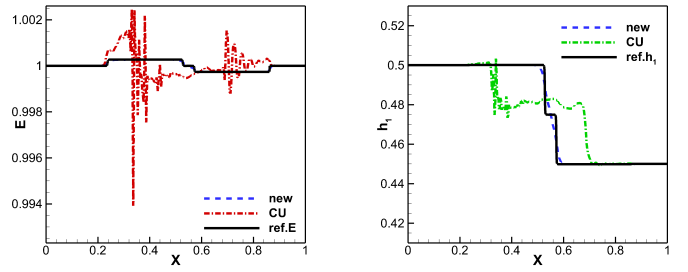

FIG. 4.9. *Interface propagation. Numerical results obtained by the new and CU scheme. Left: the total water height E; Right: the height of the upper layer h_1.*

the reference solution which is obtained by the CU scheme using 2000 uniform cells in Figure 4.8. Both the new scheme and the CU scheme can correctly reflect this complex wave pattern. The numerical results obtained by the two schemes are well in agreement.

Finally, we use 400 uniform cells to compute the numerical results using the new, CU and PCCU schemes. The PCCU scheme is proposed in [31], which can be seen as the extension of the CU scheme. We set the bottom topography function to be $B(x)=0$. We compare the numerical results with the references solutions, which are obtained by the new scheme with 10^4 uniform cells, in Figures 4.9-4.10. Only the CU scheme cannot correctly reflect this complex wave pattern. This confirms that the CU scheme depends on the reference level. The new and PCCU schemes produced similar results.

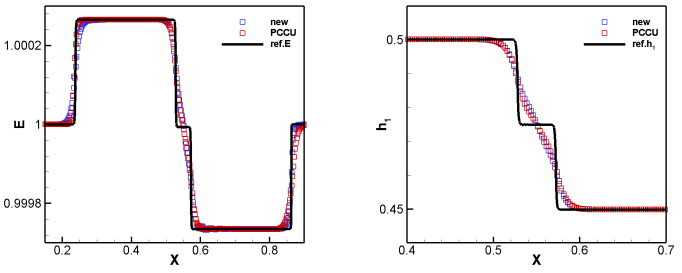

FIG. 4.10. *Interface propagation. Numerical results obtained by the new and PCCU scheme. Left: the total water level E; Right: the height of the upper layer h_1.*

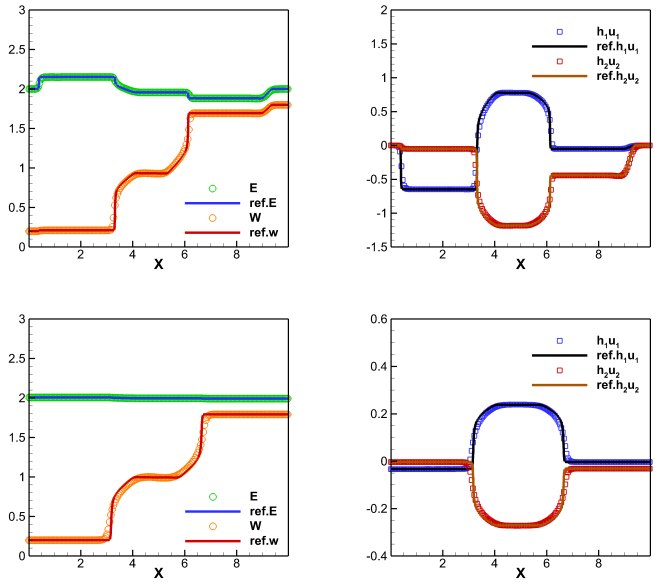

FIG. 4.11. *Unsteady flow over a flat bottom. Top left: Numerical surface and interface by the new scheme using the parameter $r=0.7$; Top right: Numerical discharge by the new scheme using the parameter $r=0.7$; Bottom left: Numerical surface and interface by the new scheme using the parameter $r=0.98$; Bottom right: Numerical discharge by the new scheme using the parameter $r=0.98$.*

4.7. Unsteady flow over a flat bottom. In this example, we consider a flat bottom $B(x)=0$. This test problem was also considered in [19, 20]. As considered in [20], if a numerical scheme lacks conservation of the total momentum, it may lead to the appearance of unphysical solutions. A wrong shock maybe produced due to the weak instability near the original discontinuity at the interface. The computation domain is [0,10].

We first set the constant density ratio is $r=0.7$, $t=1$ and the gravitational constant is $g=9.8$. The initial data is

$$h_2=\begin{cases}0.2, & \text{if } x<5,\\ 1.8, & \text{otherwise,}\end{cases} \qquad h_1=2-h_2, \quad u_1=u_2=0.$$

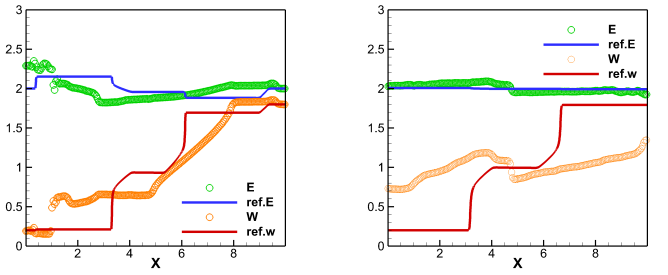

FIG. 4.12. *Unsteady flow over a flat bottom. Numerical results obtained by the CU scheme. Left:* $r=0.7$*; Right:* $r=0.98$.

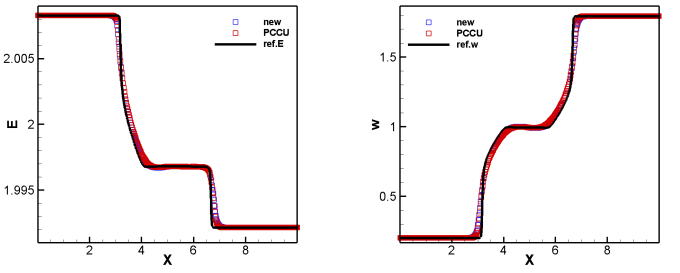

FIG. 4.13. *Unsteady flow over a flat bottom. Numerical results obtained by the new and PCCU schemes. Left: the total water level; Right: the interface.*

We run this simulation using 400 uniform cells. The numerical result is shown in Figure 4.11, one can not observe a wrong shock at the interface.

Next, we set the constant density ratio as $r=0.98$, $t=5$ and the gravitational constant is $g=9.8$. One can see that the wrong shock is not present in Figure 4.11. This confirms that the current scheme can preserve the conservation of the total momentum and is stable. We also use the CU and PCCU schemes to compute same issues. The computational results are shown in Figures 4.12-4.13, we can see that the CU scheme fails to capture the correct wave patterns. Both the new and PCCU schemes produced similar results which agree well with the reference solutions.

4.8. Small perturbation of a constant state with complex eigenvalues. This test case was discussed in [20]. The eigenvalues become to complex in this case. The constant density ratio is $r=0.98$ and the gravitational constant is $g=9.81$. The bottom topography is $B(x)=0$ and the initial data

$$h_2=\begin{cases}\frac{1}{2}+\frac{1}{100}(1+\cos(10\pi(x-5))), & \text{if } |x-5|<0.1,\\ \frac{1}{2}, & \text{otherwise,}\end{cases} \quad h_1=1-h_2,\ u_1=0.6,\ u_2=-0.6.$$

The computational domain is $[0, 10]$. The final time is $t=1$. We compute the numerical solutions using 1000 cells. One can see the computational results obtained by the new scheme and the CU scheme in Figure 4.14. The new scheme is robust and does not have large spurious oscillations. In particular, the numerical results obtained by the new scheme are still bounded.

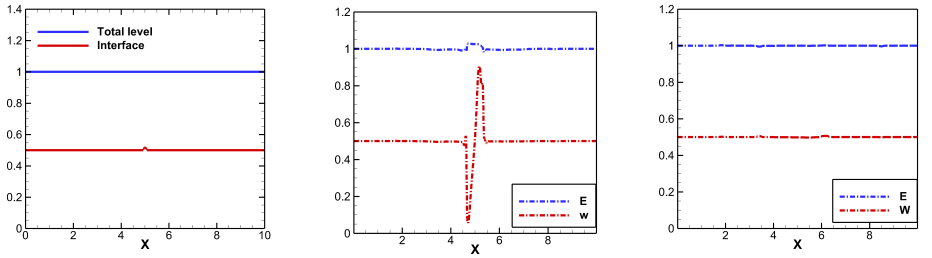

FIG. 4.14. *Small perturbation of a constant state with complex eigenvalues. Left: the initial condition; Middle: Numerical results obtained by the new scheme; Right: Numerical results obtained by the CU scheme.*

5. Conclusion

We proposed a well-balanced, positivity-preserving, second-order accurate, Godunov-type finite volume scheme based on interface hydrostatic reconstruction for the two-layer shallow water equation with wetting and drying states. We use the sub-cell reconstruction method to discretize the source term. We proved the current scheme can preserve the still water steady state solution of the system with arbitrary wet-dry fronts and is capable of preserving both layers h_1 and h_2 to be positive. Several classical problems confirm that the current scheme is robust and effective.

Acknowledgement. This work was supported in part by the Natural Science Foundation of Hunan (No.2022JJ40538) and the National Key Research and Development Plan of China (2017YFC0405901).

REFERENCES

[1] K.-A. Lie and S. Noelle, *On the artificial compression method for second-order nonoscillatory central difference schemes for systems of conservation laws*, SIAM J. Sci. Comput., 24(4):1157–1174, 2003. 2

[2] A. Bollermann, G. Chen, A. Kurganov, and S. Noelle, *A well-balanced reconstruction of wet/dry fronts for the shallow water equations*, J. Sci. Comput., 56(2):267–290, 2013. 2

[3] A. Kurganov and G. Petrova, *A second-order well-balanced positivity preserving central-upwind scheme for the Saint-Venant system*, Commun. Math. Sci., 5(1):133–160, 2007. 1

[4] T. Gallouët, J.M. Hérard, and N. Seguin, *Some approximate Godunov schemes to compute shallow-water equations with topography*, Comput. Fluids, 32(4):479–513, 2016. 1

[5] E. Audusse, F. Bouchut, M.O. Bristeau, R. Klein, and P. Benoit, *A fast and stable well-balanced scheme with hydrostatic reconstruction for shallow water flows*, SIAM J. Sci. Comput., 25(6):2050–2065, 2004. 1, 2.3

[6] P.K. Sweby, *High resolution schemes using flux limiters for hyperbolic conservation laws*, SIAM J. Numer. Anal., 21(5):995–1011, 1984. 2

[7] A. Bollermann, S. Noelle, and M. Lukáčová-Medvidová, *Finite volume evolution Galerkin methods for the shallow water equations with dry beds*, Commun. Comput. Phys., 10(2):371–404, 2011. 1

[8] S. Jin and X. Wen, *Two interface-type numerical methods for computing hyperbolic systems with geometrical source terms having concentrations*, SIAM J. Sci. Comput., 26(6):2079–2101, 2006. 2

[9] Y. Xing and C.-W. Shu, *A new approach of high order well-balanced finite volume WENO schemes and discontinuous Galerkin methods for a class of hyperbolic systems with source*, Commun. Comput. Phys., 1(1):567–598, 2006. 1

[10] S. Noelle, N. Pankratz, G. Puppo, and J.R. Natvig, *Well-balanced finite volume schemes of arbitrary order of accuracy for shallow water flows*, J. Comput. Phys., 213(2):474–499, 2006.

2
[11] G. Chen and S. Noelle, *A new hydrostatic reconstruction scheme based on subcell reconstructions*, SIAM J. Numer. Anal., 55(2):758–784, 2017. 1, 1, 2, 2.4, 3, 3
[12] M.J. Castro, P.G. LeFloch, M.L. Munoz-Ruiz, and C. Parés, *Why many theories of shock waves are necessary: Convergence error in formally path-consistent schemes*, J. Comput. Phys., 227(17):8107–8129, 2008. 2.3, 2.4, 2.5
[13] C. Parés, *Numerical methods for nonconservative hyperbolic systems: a theoretical framework*, SIAM J. Numer. Anal., 44(1):300–321, 2006. 2.3, 2.3, 2.3
[14] V. Michel-Dansac, C. Berthon, S. Clain, and F. Foucher, *A well-balanced scheme for the shallow-water equations with topography or Manning friction*, J. Comput. Phys., 335:115–154, 2017. 1
[15] X. Liu, J. Albright, Y. Epshteyn, and A. Kurganov, *Well-balanced positivity preserving central-upwind scheme with a novel wet/dry reconstruction on triangular grids for the Saint-Venant system*, J. Comput. Phys., 374:213–236, 2018. 1
[16] A. Buttinger-Kreuzhuber, Z. Horváth, S. Noelle, G. Blöschl, and J. Waser, *A new second-order shallow water scheme on two-dimensional structured grids over abrupt topography*, Adv. Water Res., 127:89–108, 2019. 1
[17] D.M. Farmer and L. Armi, *Maximal two-layer exchange over a sill and through the combination of a sill and contraction with barotropic flow*, Water Resour. Res., 164:53–76, 1986. 4.5
[18] A. Kurganov and G. Petrova, *Central-upwind schemes for two-layer shallow water equations*, Water Resourc. Res., 31(3):1742–1773, 2009. 4.1, 4.4, 4.5, 4.6
[19] F. Bouchut and T. Morales de Luna, *An entropy satisfying scheme for two-layer shallow water equations with uncoupled treatment*, ESAIM Math. Model. Numer. Anal., 42(4):683–698, 2008. 1, 4.7
[20] F. Bouchut and V. Zeitlin, *A robust well-balanced scheme for multi-layer shallow water equations*, Discrete Contin. Dyn. Syst. Ser. B, 13(4):739–758, 2010. 1, 4.2, 4.7, 4.8
[21] X. Lu, B. Dong, B. Mao, and X. Zhang, *A robust and well-balanced numerical model for solving the two-layer shallow water equations over uneven topography*, C. R. Mecanique, 343(7-8):429–442, 2015. 1
[22] R. Abgrall and K. Smadar, *Two-layer shallow water system: a relaxation approach*, SIAM J. Sci. Comput., 31(3):1603–1627, 2009. 1, 2.2
[23] M.J. Castro-Díaz, E.D. Fernández-Nieto, J.M. González-Vida, and C. Parés-Madronal, *Numerical treatment of the loss of hyperbolicity of the two-layer shallow-water system*, J. Sci. Comput., 48(1-3):16–40, 2011. 1
[24] M. Castro, J. Macías, and C. Parés, *A Q-scheme for a class of systems of coupled conservation laws with source term. Application to a two-layer 1-D shallow water system*, ESAIM Math. Model. Numer. Anal., 35(1):107–127, 2001. 1
[25] N. Izem, M. Seaid, and M. Wakrim, *A discontinuous Galerkin method for two-layer shallow water equations*, Math. Comput. Simul., 120(C):12–23, 2016. 1
[26] G. Dal Maso, Ph. Le Floch, and F. Murat, *Definition and weak stability of nonconservative products*, J. Math. Pure. Appl., 74:483–548, 1995. 1
[27] J.-J. Cauret, J.-F. Colombeau, and A.Y. Le Roux, *Discontinuous generalized solutions of nonlinear nonconservative hyperbolic equations*, J. Math. Anal. Appl., 139(2):552–573, 1989. 1
[28] A. Chiapolino and R. Saurel, *Models and methods for two-layer shallow water flows*, J. Comput. Phys., 371:1043–1066, 2018. 1
[29] C.-W. Shu and S. Osher, *Efficient implementation of essentially non-oscillatory shock-capturing schemes*, J. Comput. Phys., 77(2):439–471, 1989. 2.3
[30] J. Dong, *A robust second-order surface reconstruction for shallow water flows with a discontinuous topography and a Manning friction*, Adv. Comput. Math., 46(2):1–33, 2020. 1
[31] M.J. Castro Diaz, A. Kurganov, and T. Morales de Luna, *Path-conservative central-upwind schemes for nonconservative hyperbolic systems*, ESAIM Math. Model. Numer. Anal., 53(3):959–985, 2019. 1, 2.3, 4.6
[32] M.L. Muñoz-Ruiz and C. Parés, *Godunov method for nonconservative hyperbolic systems*, ESAIM Math. Model. Numer. Anal., 41(1):169–185, 2007. 2.3
[33] M.J. Castro, A.P. Milanés, and C. Parés, *Well-balanced numerical schemes based on a generalized hydrostatic reconstruction technique*, Math. Model. Meth. Appl. Sci., 17(12):2055–2113, 2007. 2.3, 2.3
[34] M.J. Castro Diaz, Y. Cheng, A. Chertock, and A. Kurganov, *Solving two-mode shallow water equations using finite volume methods*, Commun. Comput. Phys., 16(5):1323–1354, 2014. 1